Revista Mexicana de Astronomía y Astrofísica, **44**, 259–284 (2008)

HYDRODYNAMICAL SIMULATIONS OF THE NON-IDEAL GRAVITATIONAL COLLAPSE OF A MOLECULAR GAS CLOUD

Guillermo Arreaga-García,[1] Julio Saucedo-Morales,[1] Juan Carmona-Lemus,[2] and Ricardo Duarte-Pérez[2]

Received 2008 January 10; accepted 2008 April 3

RESUMEN

Presentamos los resultados de un conjunto de simulaciones numéricas dedicadas a estudiar el colapso gravitacional de una nube de gas interestelar, rígidamente rotante, aislada y esféricamente simétrica. Usamos una ecuación de estado barotrópica (*beos* por brevedad) que depende de la densidad de la nube ρ y que incluye una densidad crítica como parámetro libre, $\rho_{\rm crit}$. Durante el colapso temprano, cuando $\rho \ll \rho_{\rm crit}$, la *beos* se comporta como una ecuación de estado del gas ideal. Para el colapso posterior, cuando $\rho \geq \rho_{\rm crit}$, la *beos* incluye un término adicional que toma en cuenta el calentamiento del gas debido a la contracción gravitacional. Investigamos la ocurrencia de fragmentación rápida en la nube para lo cual usamos cuatro valores diferentes de la $\rho_{\rm crit}$. Trabajamos con dos tipos de modelos de colapso, de acuerdo con el perfil radial inicial de la densidad.

ABSTRACT

In this paper we present the results of a set of numerical simulations aimed to study the gravitational collapse of a spherically symmetric, rigidly rotating, isolated, interstellar gas cloud. To account for the thermodynamics of the gas we use a barotropic equation of state (*beos* for brevity) that depends on the density ρ of the cloud and includes a critical density as a free parameter, $\rho_{\rm crit}$. During the early collapse, when $\rho \ll \rho_{\rm crit}$, the *beos* behaves as an ideal gas equation of state. For the late collapse, when $\rho \geq \rho_{\rm crit}$, the *beos* includes an additional term that accounts for the heating of the gas due to gravitational contraction. We investigate the occurrence of prompt fragmentation of the cloud for which we use four different values of $\rho_{\rm crit}$. We work with two kinds of collapse models, according to the initial radial density profile: the uniform and the Gaussian clouds.

Key Words: binaries: general — hydrodynamics — ISM: kinematics and dynamics — stars: formation

1. INTRODUCTION

The star formation process begins with a strong gravitational collapse of molecular hydrogen clouds. This process increases the cloud density by several orders of magnitude, for instance, starting from 10^{-18} g cm^{-3} and ending at 10^{-1} g cm^{-3}, typical of young stellar densities (see Mathieu 1994).

Observational evidence suggests that most young stars in the Galaxy (around 50%) form in binary systems. Although with a lower frequency, it is also observed that they may group together in multiple systems having three or more stars (see Boden 2005).

Both astronomical observations and theoretical studies point to the *prompt fragmentation* of the cloud as the leading mechanism for explaining the origin and properties of binary stellar systems. The reader is referred to the review of Bodenheimer et al. (2000), where several proposed theoretical mechanisms for binary formation are discussed.

The basic idea of prompt fragmentation is that during the collapse a molecular cloud may spontaneously break into two pieces in such a way that the resulting *protostellar cores* will orbit about one another. This idea is likely to be correct if the cores

[1] Centro de Investigación en Física, Universidad de Sonora, Mexico.

[2] Gerencia de Sistemas, Instituto Nacional de Investigaciones Nucleares, Mexico.

do not undergo further fragmentation upon collapsing to higher densities. In fact, for the Taurus dark cloud, a correlation between the masses of the newly formed stars and the masses of the associated dense protostellar cores (starless) in the cloud has been observed (Myers 1983).

Thus, it is believed that the physical characteristics of the protostellar cores or of the fragments are likely to be inherited by the stars that might result from them, for instance, the ability to form stable binary or multiple systems with typical observed separations (between 1.0×10^{11} cm and 1.0×10^{16} cm) and orbital periods (ranging from a couple of days up to $10,000$ years).

Over the last two decades, a fairly large number of papers have been devoted to numerical studies of the star formation process and particularly to the collapse of an isolated uniformly rotating molecular hydrogen gas cloud (see the reviews given in Sigalotti & Klapp 2001, and Tohline 2002, and references therein). Earlier papers on collapse were largely based on low spatial resolution calculations.

However, considering that hydrodynamical flows can be very sensitive to initial conditions and that the parameter space for the initial conditions of the collapse of the cloud is huge, it is not as yet entirely clear under what conditions the fragmentation of the cloud results in a binary system of protostellar cores. It is for this reason that trusty models of the collapse process requiere a fully 3D hydrodynamical code capable of following the dynamics with an adequate resolution in order to capture the possible occurrence of prompt fragmentation. In this regard we consider that this paper may represent an improvement over earlier works in the field because: (i) we have obtained an acceptable solution for modeling the collapse (Arreaga et al. 2007, where one of us has collaborated in making a convergence study of the collapse of molecular clouds); (ii) we have followed the time evolution of the cloud beyond the occurrence of promt fragmentation, which allows us to recognize whether there have been mergers among the fragments; (iii) we have measured some physical properties of the fragments, from which we can try to understand, for instance, how the cloud original spin angular momentum gets transfered into orbital angular momentum of the resulting fragments; (iv) finally, we have measured how much mass is accreted by the resulting fragments.

In addition to the resolution requirement, there are other factors that can have a significant influence on the nature of the outcome of a given simulation, for instance, the initial radial density profile and the thermodynamics of the gas. For the former factor, we emphasize that in this paper we consider two cloud models with distinct initial radial density profiles: a uniform and a Gaussian cloud.

We include in this work the case of a uniform radial density cloud, because it has been studied very carefully by several groups since the pioneering calculations by Boss & Bodenheimer (1979). The collapse of a uniform cloud has been calculated over and over again by using different numerical techniques. This calculation has therefore acquired the status of a common test calculation for convergence testing and inter-code comparison and it has been called in the literature "the standard isothermal test case simulation."

There is good agreement among the different techniques in the outcome of the gravitational collapse of a uniform cloud: the cloud fragments into two well identified protostellar cores. This simulation has been so far the most illustrative example of the formation of a binary system.

We particularly refer to the paper by Truelove et al. (1997), which uncovers subtleties of the gravitational collapse of the uniform cloud that result from insufficient resolution in numerical simulations. Indeed, they observed the formation of a filament (a bridge connecting the protostellar cores) during an advanced phase of the collapse only when the resolution of the calculations was sufficiently high. It is now agreed that simulations prior to that of Truelove et al. (1997) may be numerically inaccurate (they failed to observe the filament) because they breached the resolution requirement.

A new generation of simulations of the collapse of the uniform cloud has been carried out since the paper by Truelove et al. (1997). We refer in particular the work by Kitsionas & Whitworth (2002) and that by Springel (2005). The resolution effect on the results of numerical simulations has been widely verified since these two groups (among others) reported the appearance of the filament.

We refer the reader to Bodenheimer et al. (2000) for a review of the most important results in the recent history of collapse calculations which have given place to great conceptual advances in the state of the art; a very interesting comparison of results obtained with codes based on different numerical techniques is also provided in that paper.

In this work we have not found any difference with regard to the recent literature concerning the collapse of the uniform density cloud. This fact allows us to trust our simulations. It is important to emphasize this point because as far as we know, no definitive solution for the collapse of the Gaussian cloud has so far been calculated.

Most calculations of the evolution of a Gaussian cloud have been done with mesh-based codes, such as the Finite Differences (FD) and Adaptive Mesh Refinement(AMR) techniques. The AMR algorithm creates a nested hierarchy of ever finer grids in fluid regions where high resolution is needed (see Balsara 2001 for a review).

In this paper we use the fully parallelized GADGET-2 code which implements the SPH (smooth particle hydrodynamics) technique. This is a Lagrangian technique in which a finite number of particles is used to sample the continuous fluid (see Monaghan 1997, 2005 for a review).

In this work we use $1,200,000$ simulation particles to model the collapse of the uniform cloud and $5,000,000$ for the Gaussian cloud. Despite the fact that with these numbers of particles we achieve enough resolution for both cloud models, it is important to mention that for the Gaussian cloud model a comparison of our results with the literature becomes a little more complicated.

Finally, let us say something about the thermodynamics of the gas. Most authors in this field have used an ideal equation of state to account for the thermodynamics of the gas. According to astronomical observations, star forming regions basically consist of molecular hydrogen clouds at 10 K. Therefore, the ideal equation of state is a good approximation for this case. However, once gravity has produced a substantial contraction of the cloud, the density reaches intermediate values, and the gas begins to heat up. In order to take this increase in temperature into account in our simulations, we have made use of a barotropic equation of state *beos*, as was proposed by Boss et al. (2000).

For instance, in the ideal gas case, the instantaneous speed of sound c_0 is constant and is equal to its average value. In the *beos* case, the instantaneous speed of sound is no longer a constant but increases with the density ρ of the cloud. However, it is still possible to define an approximate average speed of sound p/ρ by $\gamma\, c_0^2$, where γ is the effective adiabatic exponent of the gas (see § 2.3).

It should be emphasized that in order to describe correctly the transition from the ideal to the adiabatic regime, one will require solving the radiative transfer problem coupled to a fully self-consistent energy equation to obtain a precise knowledge of the dependence of temperature on density. The implementation of radiative transfer has already been included in some mesh-based codes. For particle-based codes we are only aware of the work by Whitehouse & Bate (2006), in which they studied the collapse of molecular cloud cores with an SPH code that includes radiative transfer in the flux-limited diffusion approximation. These authors showed that there are important differences in the temperature evolution of the cloud when radiative transfer is taken into account.

However, after comparing the results of our simulations with those of Whitehouse & Bate (2006) for the uniform density cloud, we conclude that the barotropic equation of state behaves in general quite well and that we can capture the essential dynamical behavior of the collapse. Despite of the fact that is indispensable to include all the detailed physics of the thermal transition in order to achieve the correct results of the collapse, we carry out these simulations because we know that there are other computational and physical factors that can have a stronger influence on the outcomes of the simulations, for instance, the total number of particles, the gravitational smoothing length, the initial conditions, among others; factors which have been more carefully taken into account in this paper.

The outline of this paper is as follows. In § 2 we explain in detail all the initial characteristics of the particle distribution that we have implemented, among others, the initial mass perturbations, and the initial energies. We also show the parameters values chosen for the GADGET-2 code. In § 3, we describe the most important characteristic of the time evolution of our simulations. We also report some of the physical properties of the resulting fragments. In § 4 we discuss the relevance of our results in view of those reported by previous investigations.

2. INITIAL CONDITIONS OF THE COLLAPSE MODELS

In this section we focus on the simulation process of gravitational collapse for both a uniform and a Gaussian (centrally condensed) clouds, see Table 1. In both cases we start with a rigidly rotating spherical cloud with radius[3] $R_0 = 4.9906939 \times 10^{16}$ cm and mass $M_0 = 1.989 \times 10^{33}$ gr. The average density of the cloud is $\rho_0 = M_0/(4/3\pi\, R_0^3) \equiv 3.82 \times 10^{-18}$ g cm^{-3}. The fact that the average density is the

[3]Equivalent to $R_0 = 0.016$ parsecs or $R_0 = 3292$ AU. The mass M_0 is equal to one solar mass.

TABLE 1

RESULTS OF COLLAPSE MODELS AND PROTOSTELLAR CORE SYSTEMS

Model	Number of Particles (millions)	$\rho_{\rm crit}$ (g cm^{-3})	Final Outcome
Uniform clouds			
UA	1.2	5.0×10^{-14}	Binary
UB	1.2	5.0×10^{-13}	Triple
UC	1.2	5.0×10^{-12}	Binary
UD	1.2	5.0×10^{-11}	Binary
Gaussian clouds			
GA	5.0	5.0×10^{-14}	Binary
GB	5.0	5.0×10^{-13}	Triple
GC	5.0	5.0×10^{-12}	Binary
GD	5.0	5.0×10^{-11}	Binary

same for both clouds will allow us to use ρ_0 to normalize the instantaneous density of the cloud during its gravitational contraction in the plots that will be presented.

2.1. *The initial radial density profile*

For the uniform cloud we follow the initial conditions used in Burkert & Bodenheimer (1993). The radial density profiles in which we are interested have the following mathematical forms:

$$\rho(r) = \rho_0 \, , \qquad \text{Uniform Cloud}$$

$$\rho(r) = \rho_c \exp(-r^2/R_c^2) \, , \qquad \text{Gaussian Cloud} \tag{1}$$

where $\rho_c = 1.7 \times 10^{-17}$ g cm^{-3} is the chosen central density; $R_c = 0.5777613699 * R_0$.

A very important point that must be emphasized is the following: (i) in Boss (1991); Boss et al. (2000) made the choice of ρ_c and R_c in such a way that the radial density profile started at $\rho(r)/\rho_0 = 20$ at $r = 0$ and ended at ρ_0 at $r = R_0$. We have abandoned this choice in this paper; instead, our initial density profile is almost 5 times greater at the center of the cloud than at its outermost region, see Figure 1.

By means of a rectangular mesh we make the partition of the simulation volume in small elements, each with a volume $\Delta x \, \Delta y \, \Delta z$; at the center of each volume we place a particle —the *i-th*, say— with a mass determined by its location according to the density profile being considered, that is: $m_i = \rho(x_i, y_i, z_i) * \Delta x \, \Delta y \, \Delta z$ with $i = 1, ..., N$.

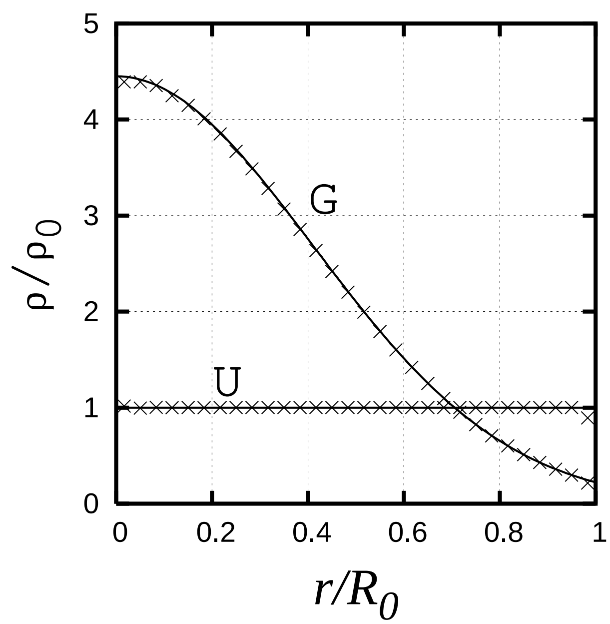

Fig. 1. Radial density profile for initial distribution of particles for both models U (Uniform cloud) and G (Gaussian cloud): The continuous curve indicates the analytical profiles and the curve with crosses indicates the measured profiles. We normalize the density with the cloud average initial density $\rho_0 = 3.82 \times 10^{-18}$ g cm^{-3} and distance with the cloud initial radius $R_0 = 4.9906939 \times 10^{16}$ cm.

Next, we displace each particle from its location a distance of the order $\Delta x/4.0$ in a random spatial direction. This is how we have obtained a set of particles reproducing the density profiles proposed by equation (1) for the initial configuration of the cloud. In fact, Figure 1 presents the initial profiles as they were numerically measured.

2.2. *Initial Energies*

The approximate total gravitational potential energy of our initial cloud of mass M_0 and radius R_0 is:

$$E_{\rm grav} \approx -\frac{3}{5}\,\frac{G\,M_0^2}{R_0}, \tag{2}$$

where G is Newton's universal gravitation constant. For an ideal gas, the average speed of sound is given by

$$\frac{p}{\rho} \equiv c_0^2 = \frac{k\,T}{\mu}, \tag{3}$$

where μ is the hydrogen molecular weight; T its equilibrium temperature and k is the Boltzmann constant. The average total energy $E_{\rm therm}$ (kinetic plus potential interaction terms of the molecules) is given by

$$E_{\rm therm} \approx \frac{3}{2}\mathcal{N}\,k\,T = \frac{3}{2}M_0\,c_0^2, \tag{4}$$

where $\mathcal{N}$ is the total number of molecules in the gas. The rotational energy of the cloud is approximately given by:

$$E_{\rm rot} = \frac{1}{2}\,I\,\Omega_0^2 = \frac{1}{2}\,\frac{J^2}{I} \approx \frac{1}{5}\,M_0\,R_0^2\,\Omega_0^2, \tag{5}$$

where $I \approx \frac{2}{5}\,M_0\,R_0^2$ is the moment of inertia; $J = I\,\Omega_0$ the total angular momentum of the cloud and Ω_0 its angular velocity.

According to the literature, the dynamical properties of the initial distribution of particles are commonly characterized by means of the thermal and rotational energy ratios with respect to the gravitational energy, α and β, respectively. For the models considered in this paper, the values of c_0 and Ω_0 are chosen (see equation 10 and equation 14) in such a way that the energy ratios are initially given the following numerical values:

$$\begin{aligned} \alpha &\equiv \frac{E_{\rm therm}}{|E_{\rm grav}|} = 0.26055 \\ \beta &\equiv \frac{E_{\rm rot}}{|E_{\rm grav}|} = 0.16134. \end{aligned} \tag{6}$$

Now, following the virial theorem, if the hydrogen cloud is in thermodynamical equilibrium, then the three previous energies satisfy the following relation:

$$2\,(E_{\rm therm} + E_{\rm rot}) + E_{\rm grav} = 0, \tag{7}$$

or, in an equivalent form,

$$\alpha + \beta = \frac{1}{2}, \tag{8}$$

a relation that will be used in the resulting plots.

2.3. *Equation of State*

In this paper we use the barotropic equation of state *beos* proposed by Boss et al. (2000):

$$p = c_0^2\rho\left[1 + \left(\frac{\rho}{\rho_{\rm crit}}\right)^{\gamma-1}\right], \tag{9}$$

where $\gamma = 5/3$ because we only consider the translational degrees of freedom of the molecular hydrogen. c_0 is the initial sound speed, whose value depends upon the initial ratio of the kinetic to the gravitational energy of the model under consideration. The values for c_0 appropriate for the α given in equation 6 of § 2.2 are:

$$\begin{aligned} c_0 &= 16647.83\ \mathrm{cm\ s^{-1}} \qquad \text{Uniform Cloud} \\ c_0 &= 19013.16\ \mathrm{cm\ s^{-1}} \qquad \text{Gaussian Cloud.} \end{aligned} \tag{10}$$

The *beos* given in equation (9) depends on a single free parameter: the critical density $\rho_{\rm crit}$. For the early phases of the collapse, when the maximum density of the cloud is much lower than the critical density, $\rho_{\rm max} \ll \rho_{\rm crit}$, the *beos* becomes an ideal equation of state, with $p \approx \rho$ and the instantaneous speed of sound is equal to its average value according to:

$$\frac{dp}{d\rho} = \frac{p}{\rho} = c_0^2. \tag{11}$$

For the late phases of the collapse, when $\rho_{\rm max} \gg \rho_{\rm crit}$, there is an increase in pressure according to $p \approx \rho^{3/2}$; the relation given in equation (11) is now only approximately valid, for in this case we have:

$$\frac{dp}{d\rho} \approx \frac{p}{\rho} \approx \gamma\,c_0^2. \tag{12}$$

We note that this thermodynamical change tries to capture the heating of the gas when the gravitational contraction is significant.

In order to study the effect of the change of regimen from low to high pressure on the outcome of the simulation we consider four values of the critical density, see Table 1.

2.4. *Initial Velocities*

Additionally, we consider that the cloud is in counterclockwise rigid body rotation around the z

axis; therefore the initial velocity of the *i-th* particle is given according to the following equation:

$$\vec{v}_i = \vec{\Omega_0} \times \vec{r}_i = (-\Omega_0\, y_i, \Omega_0\, x_i, 0), \qquad (13)$$

where Ω_0, the magnitude of the angular velocity, has been chosen according to the model under consideration to satisfy the value of β given in equation (6), see § 2.2. Thus, we have used the following two values:

$$\begin{array}{ll} \Omega_0 = 7.2 \times 10^{-13} \text{ rad s}^{-1} & \text{Uniform Cloud} \\ \Omega_0 = 1.0 \times 10^{-12} \text{ rad s}^{-1} & \text{Gaussian Cloud.} \end{array} \qquad (14)$$

2.5. *Initial Mass Perturbations*

As we are interested in the formation process of binary systems of protostellar cores, we implement a spectrum of density perturbations on the initial particle distribution, such that at the end of the simulation it might result in the formation of binary systems. This perturbation is applied to the mass of each particle m_i regardless of the cloud model according to:

$$m_i = m_0 + m_0 * a \cos(m\, \phi_i)\,, \qquad (15)$$

where m_0 is the unperturbed mass of the simulation particle, the perturbation amplitude is set to $a = 0.1$ and the mode is fixed to $m = 2$.

2.6. *Evolution Code*

We have carried out the time evolution of the initial distribution of particles with the parallel code GADGET-2, which is described in detail in Springel (2005). GADGET-2 is based on the tree-PM method for computing the gravitational forces and on the standard SPH method for solving the Euler equations of hydrodynamics.

GADGET-2 incorporates the following standard features:(i) each particle i has its own smoothing length h_i; (ii) the particles are also allowed to have individual gravitational softening lengths ϵ_i, whose values are adjusted such that for every time step $\epsilon_i\, h_i$ is of order unity.

Following Gabbasov et al. (2006), some empirical formulas are known to assign a value to ϵ_i in order to minimize errors in the calculation of the gravitational force on a particle i of mass m_i. However, GADGET-2 fixes the value of ϵ_i for each timestep using the minimum value of the smoothing length of all particles, that is, if $h_{\min} = min(h_i)$ for $i = 1, 2 ... N$, then $\epsilon_i = h_{\min}$.

In order to move the particles forward in time a complete time step $\Delta t = t^{n+1} - t^n$, GADGET-2 uses a leapfrog algorithm.

The GADGET-2 code that we have used in this paper has implemented a Monaghan-Balasara form for the artificial viscosity (Monaghan & Gingold 1983; Balsara 1995). The strength of the viscosity is regulated by setting the parameter $\alpha = 0.75$ and $\beta = 1/2 \times \alpha$, see equation (14) in Springel (2005). We have fixed the Courant factor to 0.1.

2.7. *Resolution*

Following the work in Truelove et al. (1997), the resolution requirement for a simulation to avoid the growth of numerical perturbations is expressed in terms of the Jeans wavelength λ_J, which is given by:

$$\lambda_J = \sqrt{\frac{\pi\, c^2}{G\, \rho}}. \qquad (16)$$

To obtain a form more useful for a particle based code, the resolution requirement length λ_J is written in terms of the spherical Jeans mass M_J, which is defined by

$$M_J \equiv \frac{4}{3}\pi\, \rho \left(\frac{\lambda_J}{2}\right)^3 = \frac{\pi^{\frac{5}{2}}}{6} \frac{c^3}{\sqrt{G^3\, \rho}}. \qquad (17)$$

Let us suppose that we are able to follow the collapse of the cloud until a density of (more or less) 3.0×10^{-9} g cm^{-3} has been reached. Then the minimum Jeans mass that we expect according to equation (17) is approximately given by $(M_J/M_0)_{\min} = 2.52 \times 10^{-4}$.

However, it is known that this Jeans requirement is a necessary condition to avoid the occurrence of artificial fragmentation. It is less clear whether this requirement is also a sufficient condition to guarantee the correctness of a given simulation. For instance, Bate & Burkert (1997) show that for particle based codes there is also a *mass limit resolution criterion* which needs to be fulfilled besides that of Truelove et al. (1997). They show that an SPH code produces the correct results involving self-gravity as long as the minimum resolvable mass is always less that a Jeans mass, M_J. Following Bate & Burkert (1997), the smallest mass that a SPH calculation can resolve, m_r, is equal to $m_r \approx 2 N_{\rm neigh} M_J$ where $N_{\rm neigh}$ is the number of neighboring particles included in the SPH kernel.

Therefore, the smallest mass particle m_p in our simulations must at least be such that $m_p p/m_r < 1$, where $m_r \approx M_J/80$, which gives us $m_r/M_0 = 3.15 \times$

10^{-6}. For the uniform cloud model, all simulation particles have the same mass m_p; for the simulation with $1,200,000$ particles, the ratio of the particle mass to the total mass is $m_p/M_0 = 8.3\times10^{-7}$. Comparing these mass ratios we obtain $m_p/m_r = 0.26$. For the simulation with $5,000,000$ particles we obtain $m_p/m_r = 0.063$. We conclude that all the simulation in this paper satisfy both resolution requirements, that of Truelove et al. (1997) and that of Bate & Burkert (1997).

It was demonstrated by Nelson (2006) that for 3D-SPH simulations to accurately resolve the circumstellar discs there is a resolution criterion that must be fulfilled. This criterion establishes that for the vertical structure of the disc to be well resolved the scale-height H must be greater than 4 particle smoothing lengths h at the disc mid-plane.

As was the case for the Jeans criterion, for a SPH simulation this criterion is better expressed in terms of mass rather than in terms of length; Nelson then defines the Toomre mass, which is given by $M_T = \pi\Sigma\,(\lambda_T/2)^2 = \pi\,c_s^4/G^2\,\Sigma$, where Σ is the surface density of the disc of matter; λ_T is the wavelength which defines the stability of the disc; c_s is the sound speed and G is Newton's gravitational universal constant.

We can make a rough estimate of the Toomre mass for our simulations by making use of the following approximation. Let us divide the disc height H in slices of small δz. We calculate the average volume density ρ_{av} for every slice and then the relation between surface and volume densities for every slice is $\Sigma = \rho_{av} \times \delta z$. If we consider that H for the Gaussian cloud models is approximately given by $H = 0.02 * R_0$ where R_0 is the initial radius of the cloud, then the Toomre mass is given by $M_T/M_0 = 6.0 \times 10^{-5}$. Now, following Nelson (2006), the smallest mass resolution m_r —for a simulation to prevent the appearance of numerically induced fragmentation of the disc— must be given by 6 times the average number of neighboring particles considered. Therefore, for our case we have that $m_r/M_0 \approx (M_T/M_0)/(6\times40) = 2.5\times10^{-7}$. On the other hand, as we have seen earlier the mass of the SPH particle for the simulation of $5,000,000$ particles is $m_p/M_0 = 2.0\times10^{-7}$, therefore the mass ratio which is directly related with the resolution criterion is given by $m_p/m_r = 0.8$. We conclude that at least for this rough estimate our simulations have enough mass resolution also for the disc. Obviously, this claim must be taken with caution until a complete study can be properly undertaken.

3. RESULTS

In order to study the results of the simulations in this paper, we plot iso-density curves for a slice of particles around the equatorial plane of the cloud. A bar located at the bottom of these plots shows the range of values for the log of the density $\rho(t)$ at time t normalized to the average initial density (that is $\log_{10}(\rho/\rho_0)$) and the color allocation set by the program pvwave version 8. According to this color scale, yellow indicates the areas with higher densities, whereas blue indicates those with lower densities; green and orange indicate the intermediate density areas.

There is a characteristic time scale relevant[4] to the time evolution of the cloud: the free fall time $t_{\rm ff}$ (the time for a particle to reach the center of the cloud):

$$t_{\rm ff} \approx \sqrt{\frac{3\,\pi}{32\,G\,\rho_0}} = 1.07488\times10^{12}\,\mathrm{s} \approx 3.4\times10^4\ \mathrm{yr} \tag{18}$$

We take advantage of the fact that the free fall time is the same for both the uniform and the Gaussian cloud in order to normalize the time evolution with $t_{\rm ff}$.

The mass of the initial cloud is much greater than the Jeans mass, $M_0 \gg M_J$, for the collapse to begin. Numerical simulations performed so far have proved that this rotating molecular cloud contracts to an almost flat configuration in less than a free fall time $t_{\rm ff}$ of dynamical evolution. It is less clear under what conditions this flat configuration fragments. Furthermore, in case this fragmentation occurs, how likely is it that the outcome will turn out to be a binary or a multiple system? In the case of a multiple system, it is not known which are the most relevant dynamical properties of the resulting fragments, for instance, the mass, separation, orbital periods and angular momenta. These are the kind of questions we look forward to consider in the following sections of this paper.

The main results of this paper are therefore contained both in the isodensity plots and in the plots of integral properties of the resulting fragments where we show the time evolution of some physical properties of the protostellar cores. In order to calculate the physical properties of fragments we have introduced a numerical definition, which is given in the Appendix A.

[4]The orbital period of rotation around the axis of symmetry, $t_{\rm rot}$, is not relevant because it is very large $2\pi/\Omega_0 \approx 5.8t_{\rm ff}$ compared with $t_{\rm ff}$ and t_s. So, the important features of the time evolution occur before a complete orbital revolution is reached.

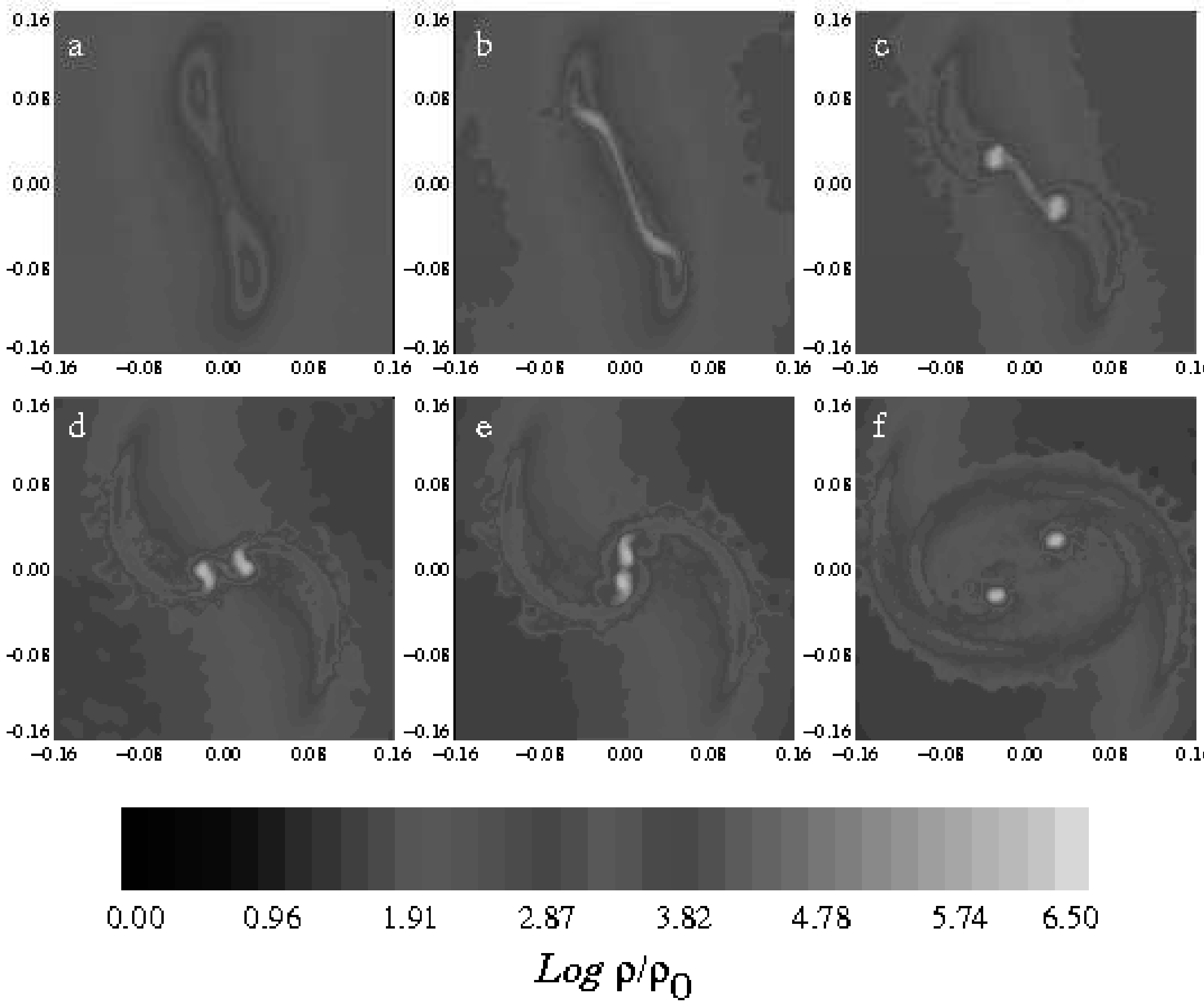

Fig. 2. Isodensity curves of the cloud midplane for model UA when the distribution of particles reaches a peak density of (a)$\rho_{\max} = 5.314 \times 10^{-14}$ g cm^{-3} at time $t/t_{\rm ff} = 1.2626$; (b)$\rho_{\max} = 7.364 \times 10^{-13}$ g cm^{-3} at time $t/t_{\rm ff} = 1.2897$; (c)$\rho_{\max} = 3.502 \times 10^{-12}$ g cm^{-3} at time $t/t_{\rm ff} = 1.3212$; (d)$\rho_{\max} = 5.110 \times 10^{-12}$ g cm^{-3} at time $t/t_{\rm ff} = 1.3437$; (e)$\rho_{\max} = 7.440 \times 10^{-12}$ g cm^{-3} at time $t/t_{\rm ff} = 1.3549$ and (f)$\rho_{\max} = 1.361 \times 10^{-11}$ g cm^{-3} at time $t/t_{\rm ff} = 1.3954$.

3.1. *The Uniform Cloud Models*

In this section we show the main results for the uniform models: For model UA see Figures 2 and 3; for model UB see Figures 4 and 5; for model UC see Figures 6 and 7 and finally for model UD see Figures 8 and 9. Below we give a more detailed explanation of each model.

Due to the fact that the centrifugal force along the equator of the cloud is grater than at the poles, the contraction of the cloud is faster along the rotation axis, and the cloud starts evolving through a sequence of flatter configurations.

When the evolution time is almost a free fall time, the cloud has lost its initial spherical symmetry, because most of the particles have found a place in a narrow slice of matter around the equatorial plane. From the point of view of the rotation axis, the accretion of particles takes place with cylindrical symmetry. During this first stage of gravitational contraction, the cloud has reduced its dimensions to 10% of its original size.

Later on, when the flattening of the cloud is extreme, the central part becomes slightly stretched taking the form of a prolate ellipsoid (Figure 6a and Figure 6b). As long as the cloud continues rotat-

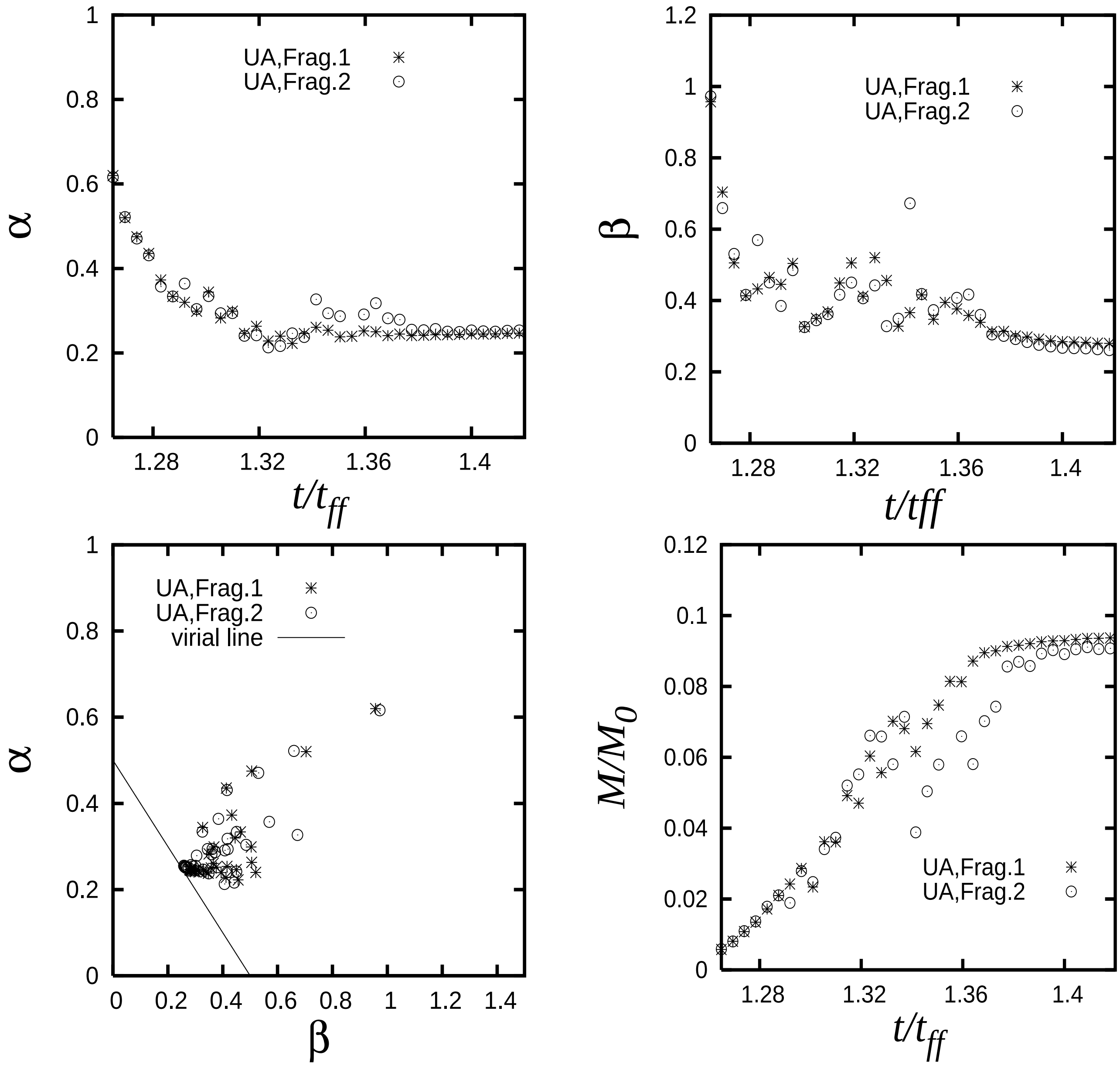

Fig. 3. Integral properties for the fragments found in models UA.

ing, the central part will adopt a more elongated and slightly curved configuration. We then notice the appearance of two small overdense cores in each extreme of the prolate central region (Figure 2a and Figure 4a). Shortly after, we note that these small cores get connected by a very well defined bridge of particles. At that moment, it is adequate to define these small overdensity cores as protostellar fragments.

Up to this point, the evolution of all uniform models proceeds in an identical fashion. What happens to the bridge of particles connecting the fragments is what makes the difference in the subsequent evolution of the uniform models; that is, the bridge will disappear or will become a thin filament.

For instance, in the UA model the change in the thermodynamics regime occurs earlier than in the other models, when $\rho_{\max} > \rho_{\rm crit} = 5.0 \times 10^{-14}$ g cm^{-3}, the pressure of the barotropic equation of state ($p \approx \rho_{\max}^{3/2}$) is greater than the pressure in the ideal equation of state ($p \approx \rho_{\max}$) for a given density. The increase in pressure slows down the gravitational

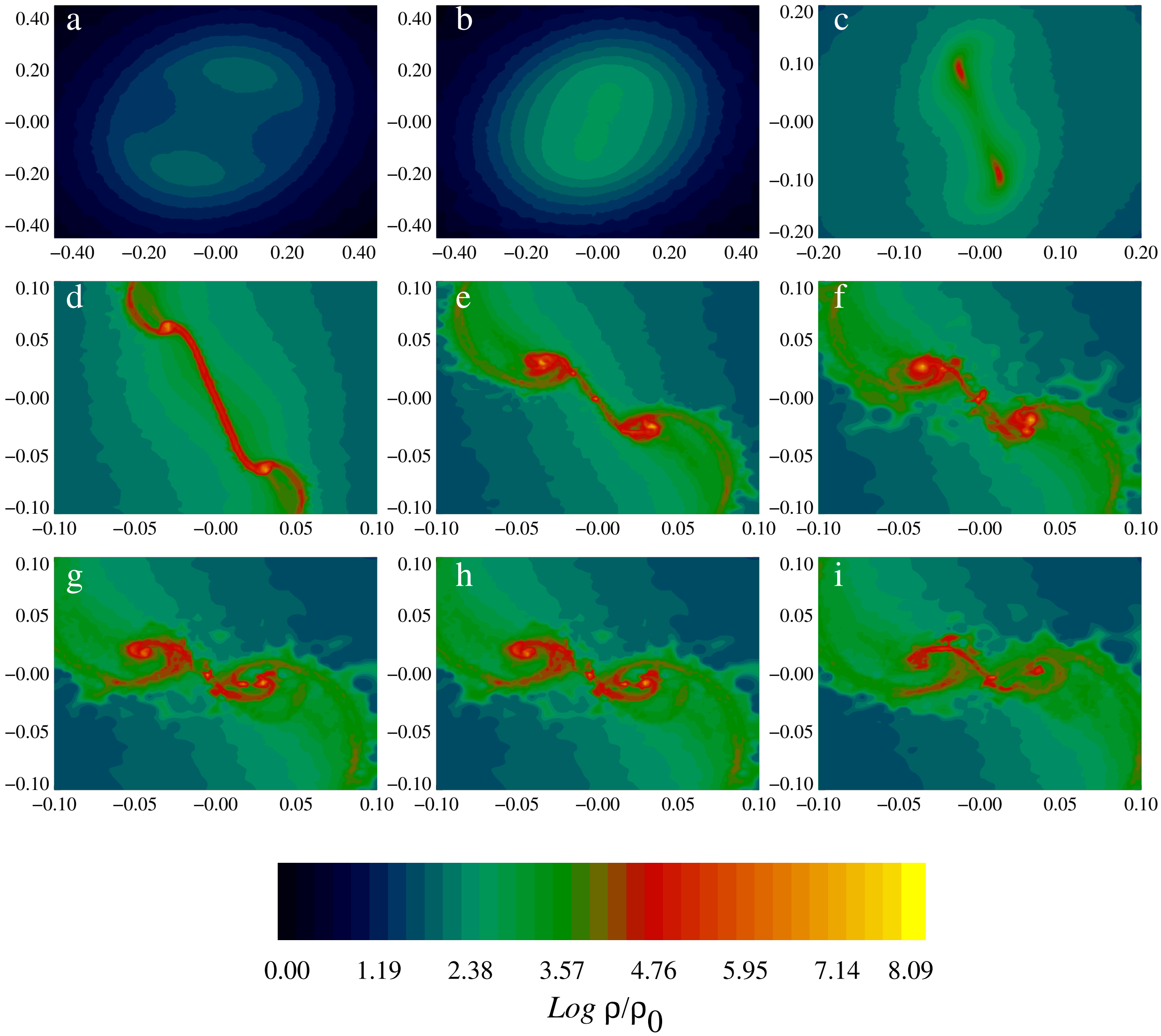

Fig. 4. Isodensity curves of the cloud mid-plane for model UB when the distribution of particles reaches a peak density of (a)$\rho_{\rm max} = 4.3640757 \times 10^{-16}$ g cm^{-3} at time $t/t_{\rm ff} = 1.084881$; (b)$\rho_{\rm max} = 1.7800040 \times 10^{-15}$ g cm^{-3} at time $t/t_{\rm ff} = 1.129897$; (c)$\rho_{\rm max} = 6.4807202 \times 10^{-13}$ g cm^{-3} at time $t/t_{\rm ff} = 1.260443$; (d)$\rho_{\rm max} = 5.1288698 \times 10^{-11}$ g cm^{-3} at time $t/t_{\rm ff} = 1.287452$; (e)$\rho_{\rm max} = 4.4799 \times 10^{-10}$ g cm^{-3} at time $t/t_{\rm ff} = 1.318963$; (f)$\rho_{\rm max} = 5.7860 \times 10^{-10}$ g cm^{-3} at time $t/t_{\rm ff} = 1.3233$; (g)$\rho_{\rm max} = 6.8657612 \times 10^{-10}$ g cm^{-3} at time $t/t_{\rm ff} = 1.334179$; (h)$\rho_{\rm max} = 7.1663927 \times 10^{-10}$ g cm^{-3} at time $t/t_{\rm ff} = 1.334179$ and (i)$\rho_{\rm max} = 7.4082296 \times 10^{-10}$ g cm^{-3} at time $t/t_{\rm ff} = 1.340301$.

collapse of both fragments. In spite of this, the fragments continue accreting matter from the surroundings, although at a smaller rate.

It is noticeable that the bridge of particles begins to disappear because the fragments accrete the particles of the bridge as well. Influenced by pure gravitational attraction among the fragments, they get closer and closer together, even to the point of touching, but they do not merge, continuing their individual trajectories until finally they enter into orbit with one another, see Figure 2f.

We observe that the UA model results in a stable binary system of protostellar fragments. Besides, in Figure 3 it is clearly observed that these fragments have a tendency to virialize. These figures suggest that the subsequent virialization of the fragments is basically accomplished by means of the rotational energy ($\beta \approx 1/2$).

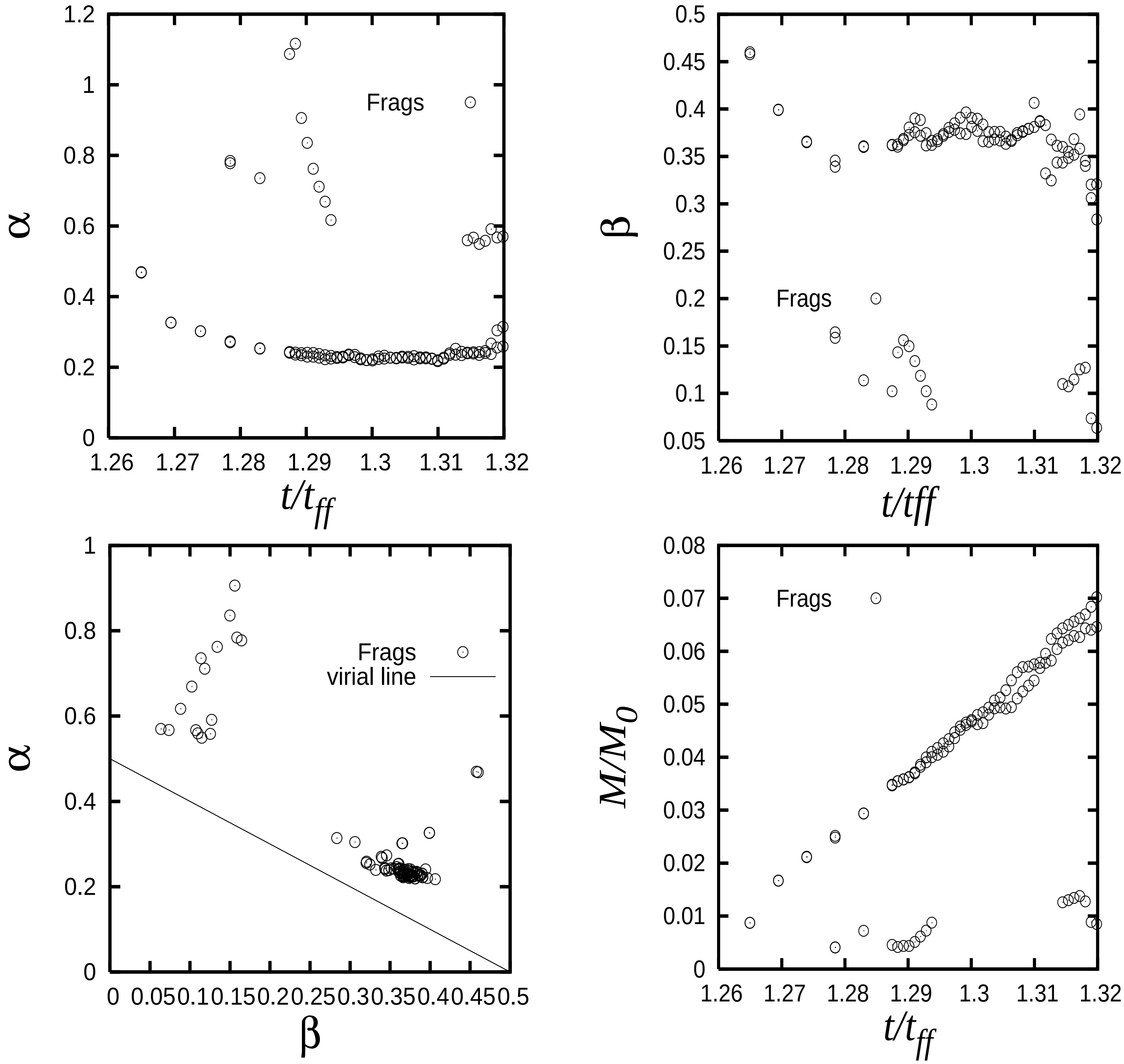

Fig. 5. Integral properties for the fragments found in models UB.

For the uniform cloud models when the change in the equation of state occurs later, for instance, models UC and UD, the final configuration is a very thin filament that connects two small overdensity cores, see Figures 6 and 8. For both UC and UD models, the cores also present a lengthening in such a way that they become aligned with the filament.

To be sure that there are no artificial effects possibly caused by extrapolation errors when the isodensity curves are generated with the pvwave program, we include in Figure 10 the configuration of particles (a dot represents a single simulation's particle).

For model UC, cylindrical symmetry can be appreciated for the cores, as well as the smooth connection of the cores and the filament through the formation of small spiral arms. We never observe fragmentation, neither in the cores nor in the filament.

However, it is possible that for model UD some breakage is already taking place in the region between the filament and the cores (see Figure 10b).

Finally, we show in Figure 11 the time evolution of the maximum density for each uniform model. We

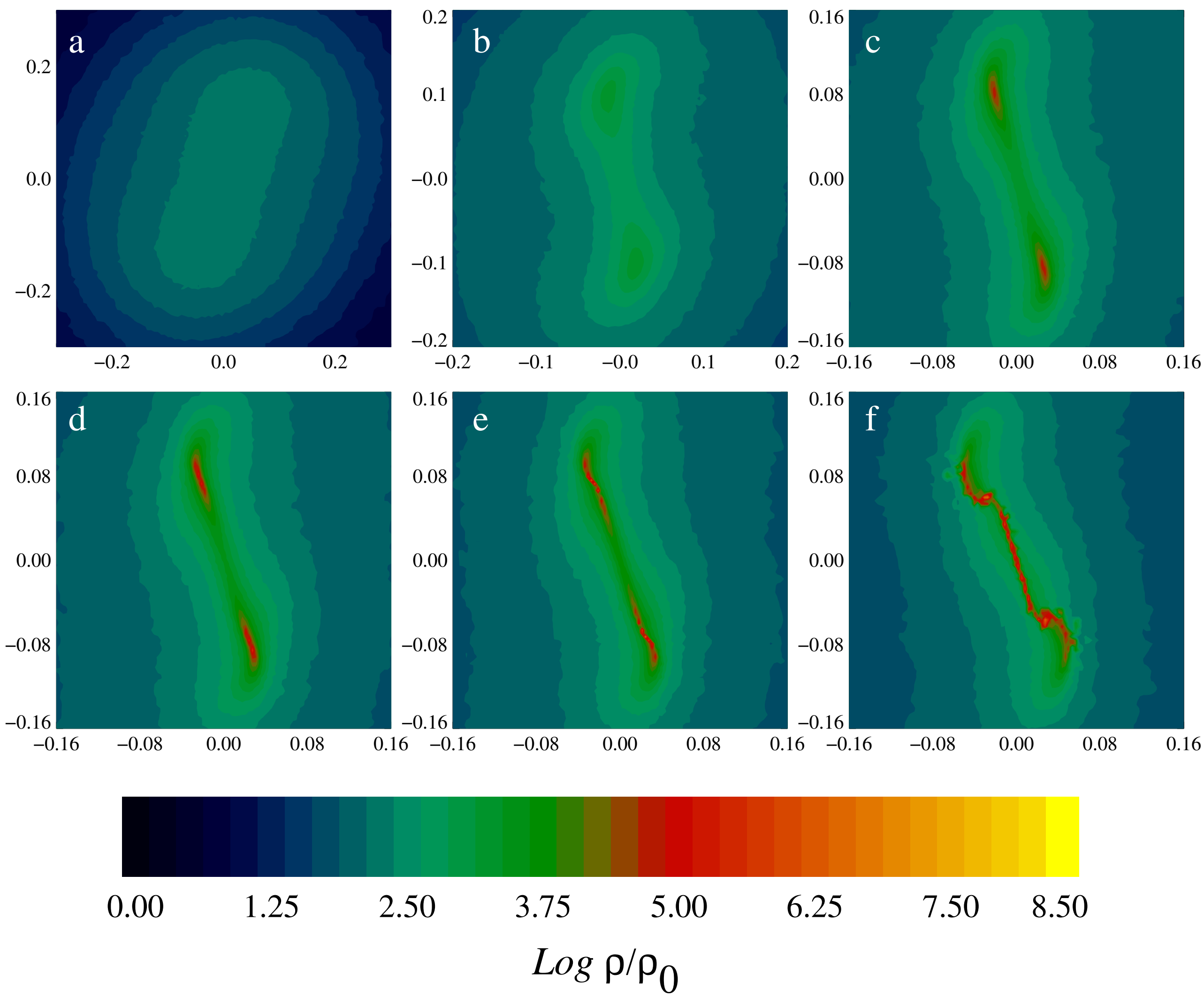

Fig. 6. Isodensity curves of the cloud mid-plane for model UC when the distribution of particles reaches a peak density of (a)$\rho_{\rm max} = 9.80 \times 10^{-16}$ g cm^{-3} at time $t/t_{\rm ff} = 1.1146$; (b)$\rho_{\rm max} = 9.37 \times 10^{-15}$ g cm^{-3} at time $t/t_{\rm ff} = 1.2460$; (c)$\rho_{\rm max} = 4.19 \times 10^{-13}$ g cm^{-3} at time $t/t_{\rm ff} = 1.2658$; (d)$\rho_{\rm max} = 6.93 \times 10^{-12}$ g cm^{-3} at time $t/t_{\rm ff} = 1.2694$; (e)$\rho_{\rm max} = 6.74 \times 10^{-10}$ g cm^{-3} at time $t/t_{\rm ff} = 1.2748$ and (f)$\rho_{\rm max} = 5.96 \times 10^{-09}$ g cm^{-3} at time $t/t_{\rm ff} = 1.2910$.

observe that the maximum density for model UA reaches its peak value and presents a tendency to remain around that maximum value; this behavior suggests a deceleration of the collapse of the cloud. For models UC and UD, it is evident that the cloud keeps collapsing without decelerating even at the most advanced stage of evolution with densities as high as 5.0×10^{-7} g cm^{-3}.

3.2. *The Gaussian Cloud Models*

In this section we show the main results for the Gaussian models: For model GA see Figures 12 and 13; for model UB see Figures 14 and 15; for model UC see Figures 16 and 17 and finally for model UD see Figures 18 and 19. Below we give a more detailed explanation of each model.

In the Gaussian models we have also introduced an initial perturbations density profile that induces the formation of binary systems, see equation (15). However, for the Gaussian cloud this perturbation is less influential on the subsequent development of the collapse than for the case of the uniform cloud. Due to the exponentially falling radial density profile of the Gaussian models, the density of the central region is almost 5 times higher than in the external regions of the cloud; for this reason the collapse takes place first in the central regions and, subsequently,

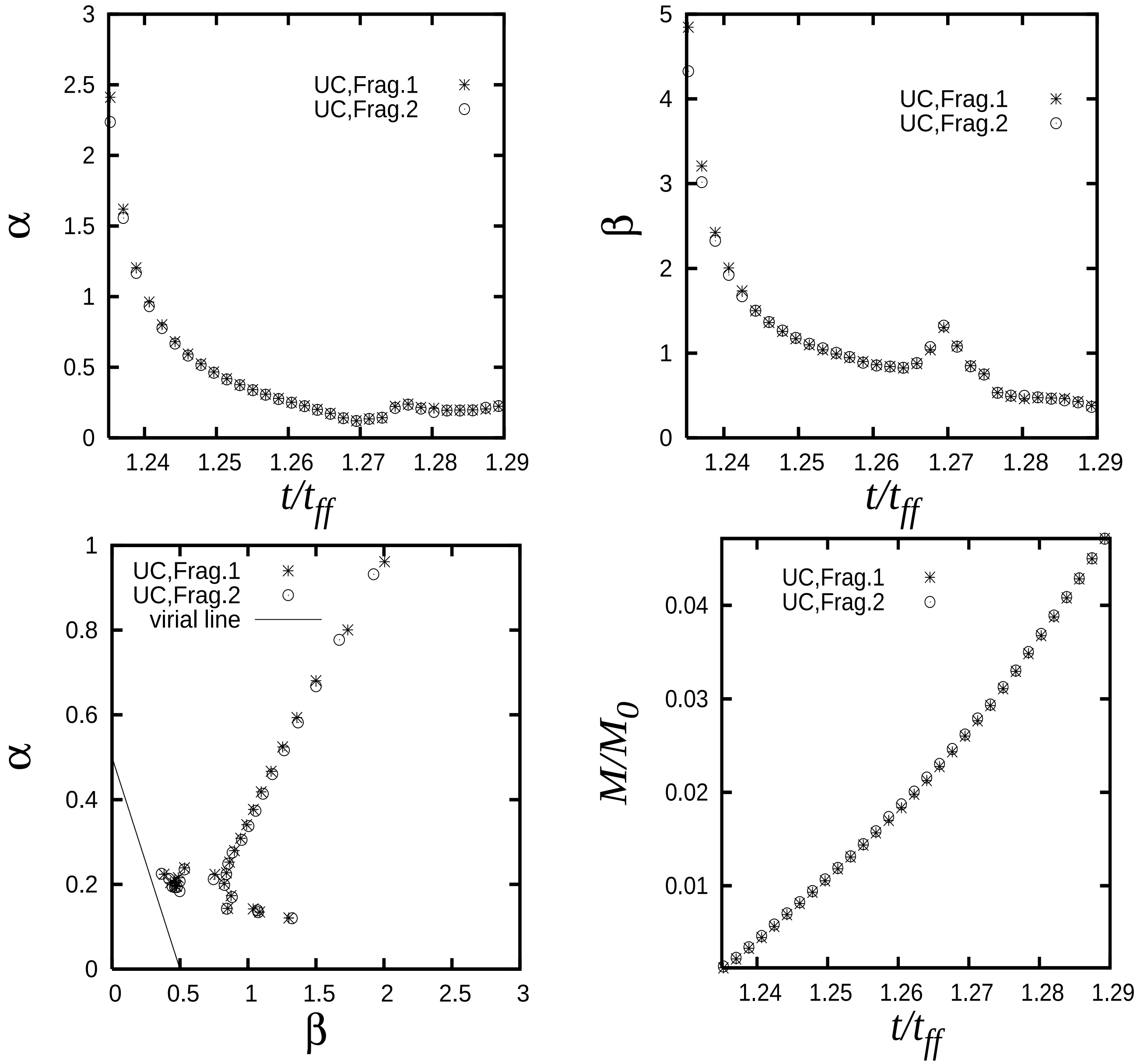

Fig. 7. Integral properties for the fragments found in models *UC*.

the collapse continues by accreting particles of the outermost regions.

It can be appreciated from the axis of rotation that the cloud conserves a circular shape (cylindrical symmetry) during the first stage of the collapse. Keeping this axial symmetry, the maximum density in the center of the cloud can reach values that are even higher than $\rho_{\max} \approx 1.0 \times 10^{-13}$ g cm^{-3}, which are observed at time $t/t_{\rm ff} \approx 0.67$, while its spatial dimensions have already been reduced by 80% for all Gaussian models.

Shortly after, the central clump of the cloud begins to rapidly change its geometry acquiring the characteristic elongated structure of bars (see for instance Figure 12a and Figure 14a).

For the Gaussian cloud, we must compare the output of our simulations with the work by Boss et al. (2000), in which they considered the collapse of a Gaussian cloud, but using an Adaptive Mesh Refinement (AMR) technique with a very high spatial resolution.

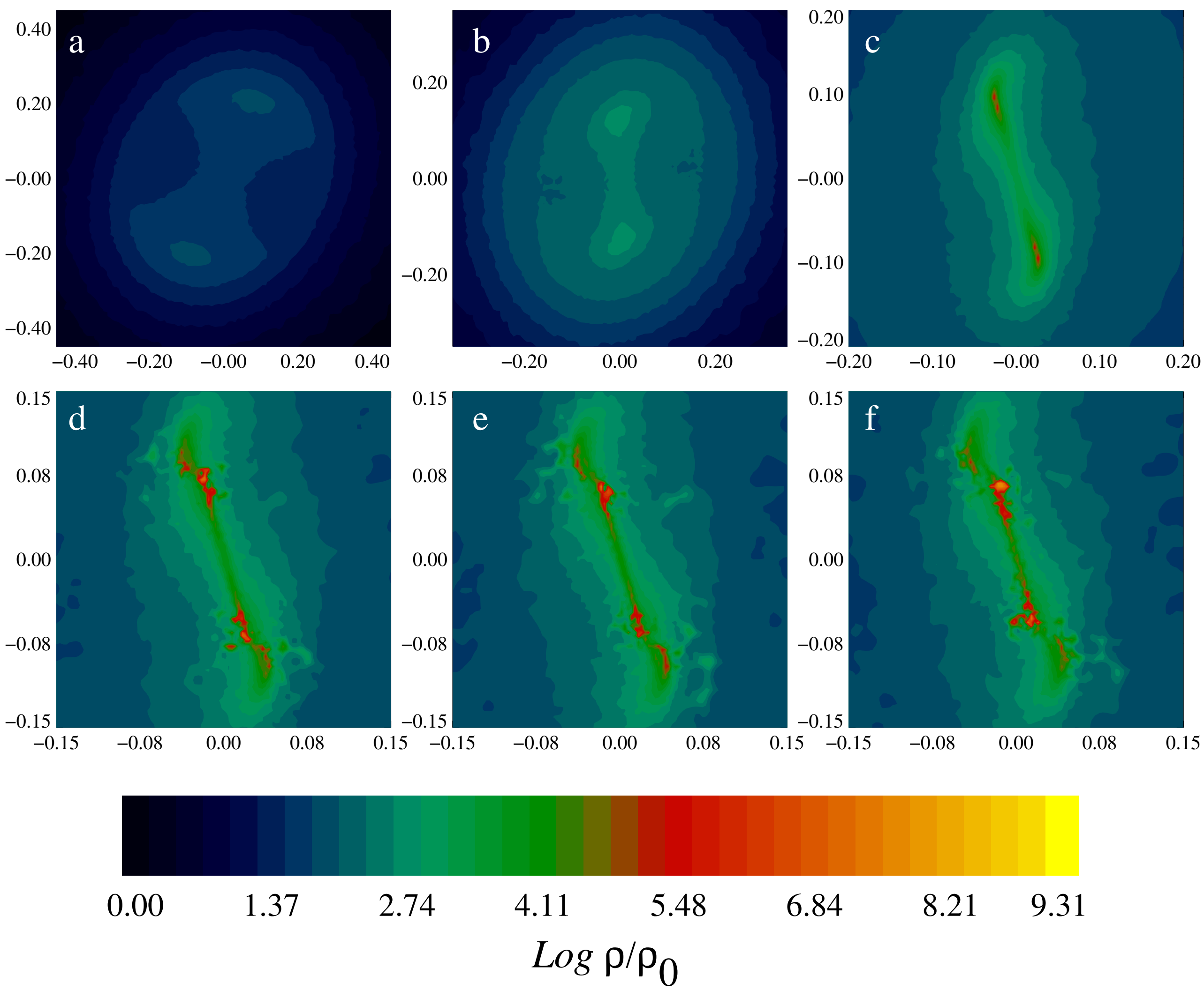

Fig. 8. Isodensity curves of the cloud mid-plane for model UD when the distribution of particles reaches a peak density of (a)$\rho_{\rm max} = 3.5817632 \times 10^{-16}$ g cm^{-3} at time $t/t_{\rm ff} = 1.08038$; (b)$\rho_{\rm max} = 2.9998504 \times 10^{-15}$ g cm^{-3} at time $t/t_{\rm ff} = 1.215427$; (c)$\rho_{\rm max} = 6.9658080 \times 10^{-11}$ g cm^{-3} at time $t/t_{\rm ff} = 1.260443$; (d)$\rho_{\rm max} = 2.2228403 \times 10^{-07}$ g cm^{-3} at time $t/t_{\rm ff} = 1.271697$; (e)$\rho_{\rm max} = 2.8109875 \times 10^{-07}$ g cm^{-3} at time $t/t_{\rm ff} = 1.273948$ and (f)$\rho_{\rm max} = 3.0019162 \times 10^{-07}$ g cm^{-3} at time $t/t_{\rm ff} = 1.276198$.

Additionally, long spiral arms form around the central bar by the effect of cloud rotation. In Figure 12b we show the extension of the spiral arms with regard to the size of the bar. It is noteworthy that Figure 12a agrees well with Figure 5a in Boss et al. (2000), even though the extension of the spiral arms in their paper cannot be clearly appreciated.

Up to this time, the evolution of all the Gaussian models are practically the same. The subsequent evolution of the central bar is what makes the most significant difference in the dynamical evolution among these models.

For instance, in model GA, in which the barotropic thermodynamics enters early in the collapse, we observe the notable occurrence of the decay and the subsequent fragmentation of the central bar. In fact, the bar in this model breaks up at its center producing two fragments. In Figure 12 we show isodensity curves where the initial formation stage of two well defined clumps located on the extremes of the bar can be appreciated; we make this snapshot when the cloud has reached a maximum density of $\rho_{\rm max} = 4.2 \times 10^{-12}$ g cm^{-3}. These clumps will provoke shortly the fragmentation of the bar. Our Figure 12 can indeed be compared with Figures 3, 5a

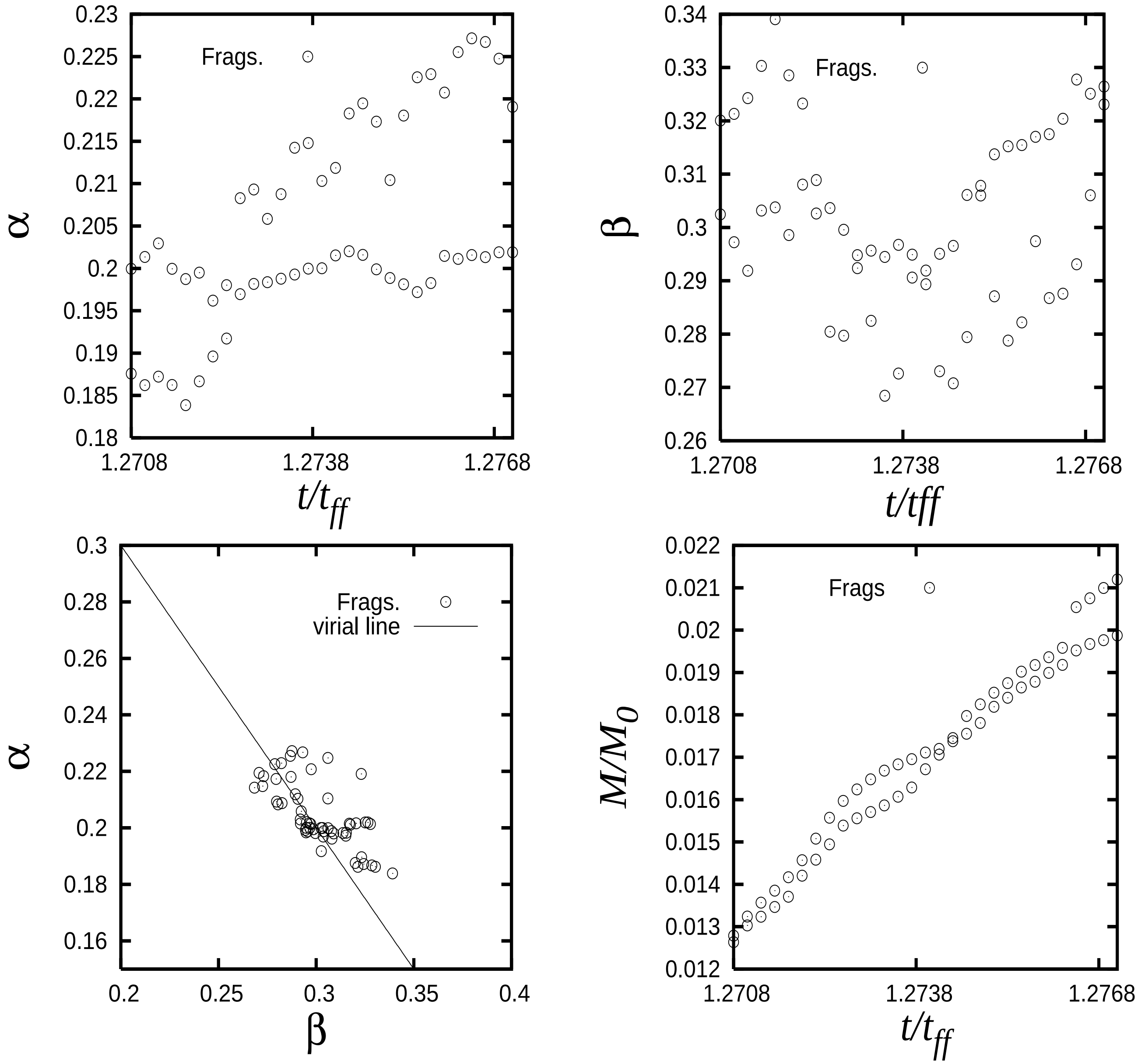

Fig. 9. Integral properties for the fragments found in models UD.

and 5b of Boss et al. (2000), in which they used isodensity curves to illustrate the geometry of the bar in its rotational movement (see their Figures 2 and 5a). In our case, the formation of the two clumps at the extremes of the bar can also be perfectly appreciated and compared with their Figure 5b.

It should be noticed that the two exterior fragments resulting from the breakage of the spiral arms are already present at the time when the fragmentation of the bar occurs. Then, at this time, the result of the simulation is four fragments. Shortly thereafter, the occurrence of merging between two fragments leaves only two final fragments that go into orbit until they reach virial equilibrium (see Figure 13).

We should emphasize that except for the formation of the bar, the dynamical evolution we observe is different from the one shown in Figure 5d of Boss et al. (2000). These authors reported that the bar decayed rapidly into a single central clump surrounded by long spiral arms. They did not mention anything about the breakage of the long spiral arms that we have observed.

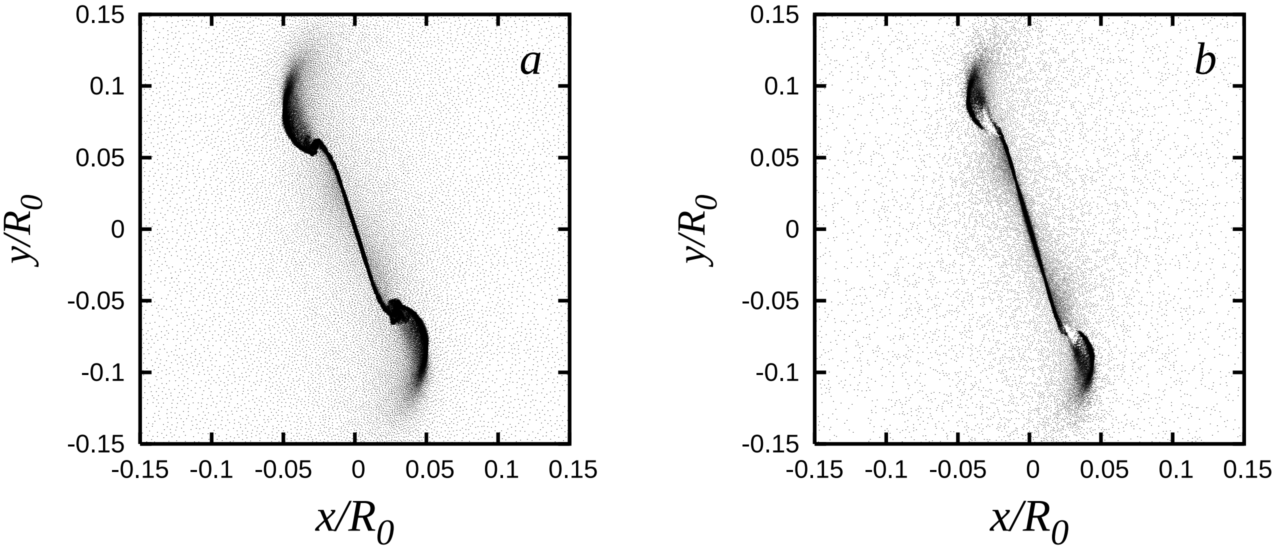

Fig. 10. Position of particles lying within a slice of thickness $\Delta z = 5.0 \times 10^{-4}$ about the equator of the cloud for Models (a) UC for maximum density 3.60×10^{-9} g cm^{-3} at time $1.286 t_{\rm ff}$ and (b) UD for maximum density $2.8596622 \times 10^{-07}$ g cm^{-3} reached at $1.276649 t_{\rm ff}$.

Boss et al. (2000) considered the value $\rho_{\rm crit} = 3.16 \times 10^{-12}$ g cm^{-3}, which is slightly smaller that the value we used in the model GC and is greater than the value we used in model GD. They observe that the Gaussian cloud fragments into a binary protostar system, but these binary clumps soon thereafter evolve into a central clump surrounded by spiral arms containing two more clumps. What we observe in model GC is that the central bar indeed fragments into two clumps; but during the time that we have followed the collapse we do not observe the merging of these clumps, neither in model GC nor in model GD. It is more likely that merging will occur in model GD than in model GC. Had we observed the merging of these fragments, we would have claimed that our simulation agreed with that of Boss et al. (2000) despite the fact that our initial density profile was not the same.

As was the case for the run GA, in model GB the central region starts deforming smoothly and it quickly adopts the elongated shape characteristic of the bars. The bar rotation provokes the appearance of spiral arms. The arms are short-sized at the beginning; but they stretch out as the rotation speed of the central bar increases. As was previously the case, these spiral arms break up, separating from the central fragment, and produce a couple of exterior fragments (see Figure 14).

The bar continues to deform by the effect of tidal forces until at some point it begins to return to

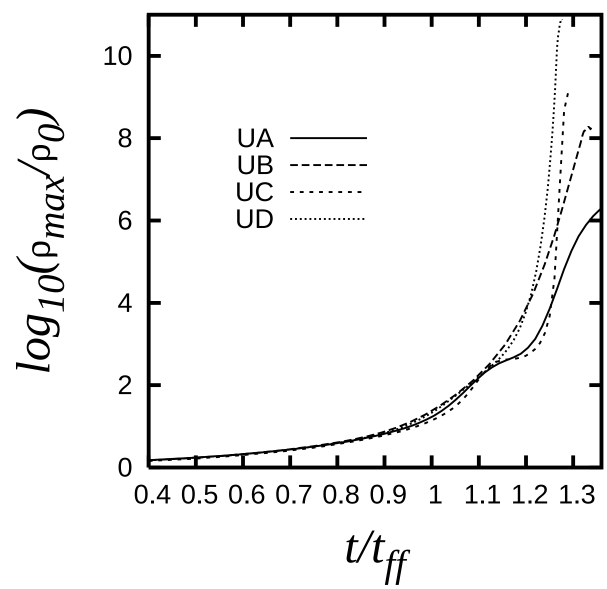

Fig. 11. Time evolution of the peak density for uniform models.

the axisymmetric (circular) configuration, presumably increasing its rotation speed. As a consequence, new spiral arms develop around the central fragment (see Figure 14). Again, when the difference in the rotation speed is high enough, a new breakage of the younger spiral arms occurs. We have therefore a multiple system of 4-well defined fragments orbiting among themselves. However, we never observe the

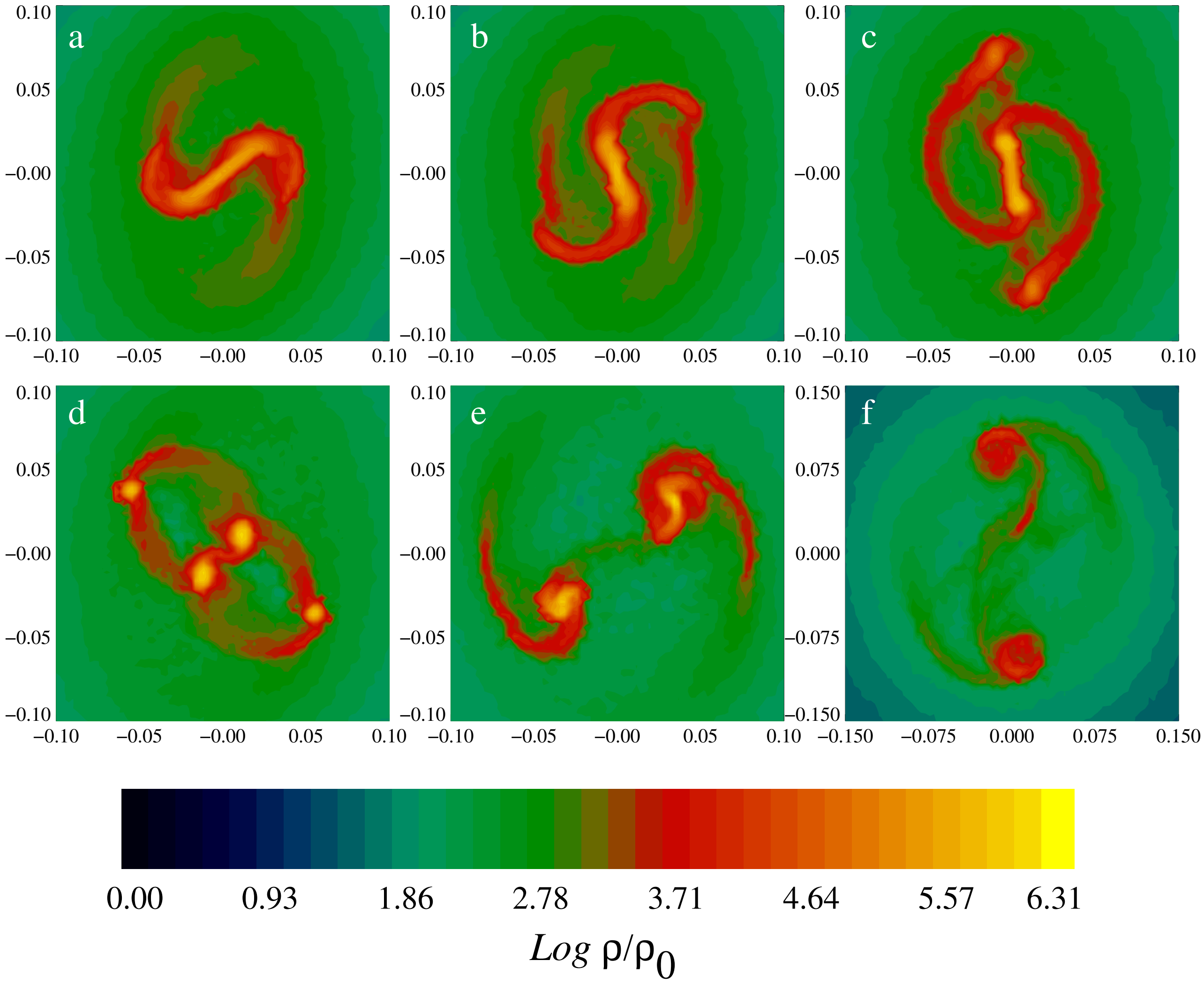

Fig. 12. Isodensity curves of the cloud mid-plane for model GA when the distribution of particles reaches a peak density of (a)$\rho_{\rm max} = 1.7959198 \times 10^{-12}$ g cm^{-3} at time $t/t_{\rm ff} = 0.747263$; (b)$\rho_{\rm max} = 3.3803476 \times 10^{-12}$ g cm^{-3} at time $t/t_{\rm ff} = 0.765269$; (c)$\rho_{\rm max} = 3.6623149 \times 10^{-12}$ g cm^{-3} at time $t/t_{\rm ff} = 0.792278$; (d)$\rho_{\rm max} = 8.1708079 \times 10^{-12}$ g cm^{-3} at time $t/t_{\rm ff} = 0.819288$; (e)$\rho_{\rm max} = 1.6487187 \times 10^{-11}$ g cm^{-3} at time $t/t_{\rm ff} = 0.864304$ and (f)$\rho_{\rm max} = 2.7573437 \times 10^{-11}$ g cm^{-3} at time $t/t_{\rm ff} = 0.927326$.

fragmentation of the central bar as was the case in model GA.

It is important to point out that the external fragments rapidly accumulate mass, which mostly comes from the remainders of the spiral arms; for instance, Figures 13 and 15 illustrate this accretion process. The resulting fragments do not virialize completely, as can be appreciated in Figures 17 and 19. These figures indeed suggest that the collapse of the fragments is still in progress, but we have not followed the subsequent time evolution because the time-step of the run becomes extremely small, to the point of being almost incapable to move the simulation particles forward in time.

Finally, we show in Figure 20 the time evolution of the peak density for each Gaussian model.

4. CONCLUDING REMARKS

One of the mechanisms proposed so far to explain the formation of binary stars is *prompt fragmentation*. The basic idea of this mechanism is that during the collapse of an isolated rotating molecular gas cloud, it may spontaneously break up into two fragments that enter into a stable orbit about one another.

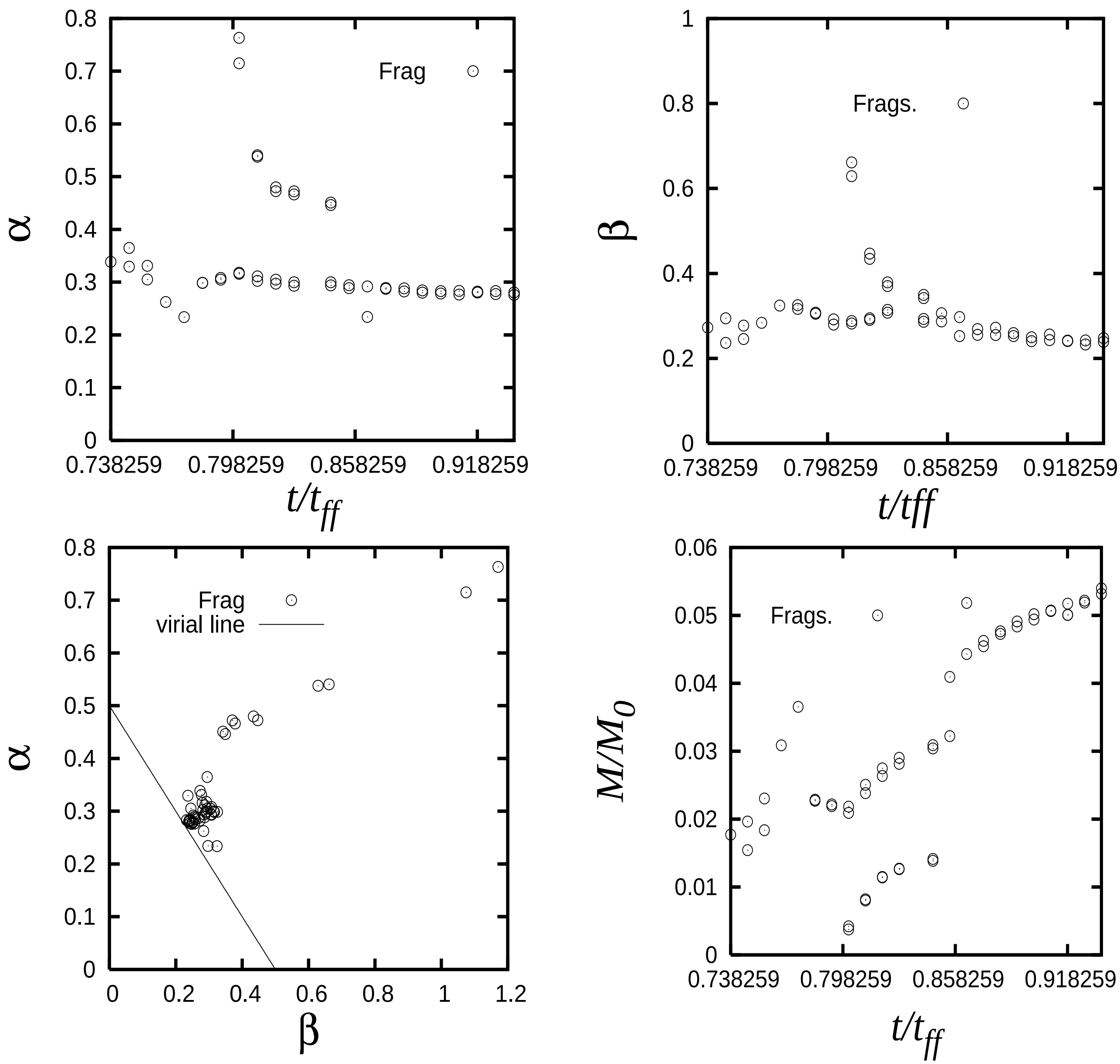

Fig. 13. Integral properties for the fragments found in models *GA*.

In order to study theoretically the sensitivity of this mechanism to the non-ideal nature of the collapse, we carried out in this paper a fully three dimensional set of numerical hydrodynamical simulations at high spatial resolution aimed to model the gravitational collapse of both uniform and Gaussian clouds with a barotropic equation of state within the framework of the SPH technique.

4.1. *The Uniform Cloud*

We emphasize that our simulations of the uniform cloud can follow the collapse to the maximum density and evolution time shown in Table 2. We have not found any difference with regard to the literature concerning the collapse of the uniform cloud, for instance, see Kitsionas & Whitworth (2002).

In all the uniform models we observe as a result the formation of a binary system of protostellar fragments that are connected by a filament, irrespective of the value of the critical density. The properties of the fragments, the mass, the radius, the α and β ratios and the properties of the filament, strongly depend on the critical density, as can be seen in Table 3.

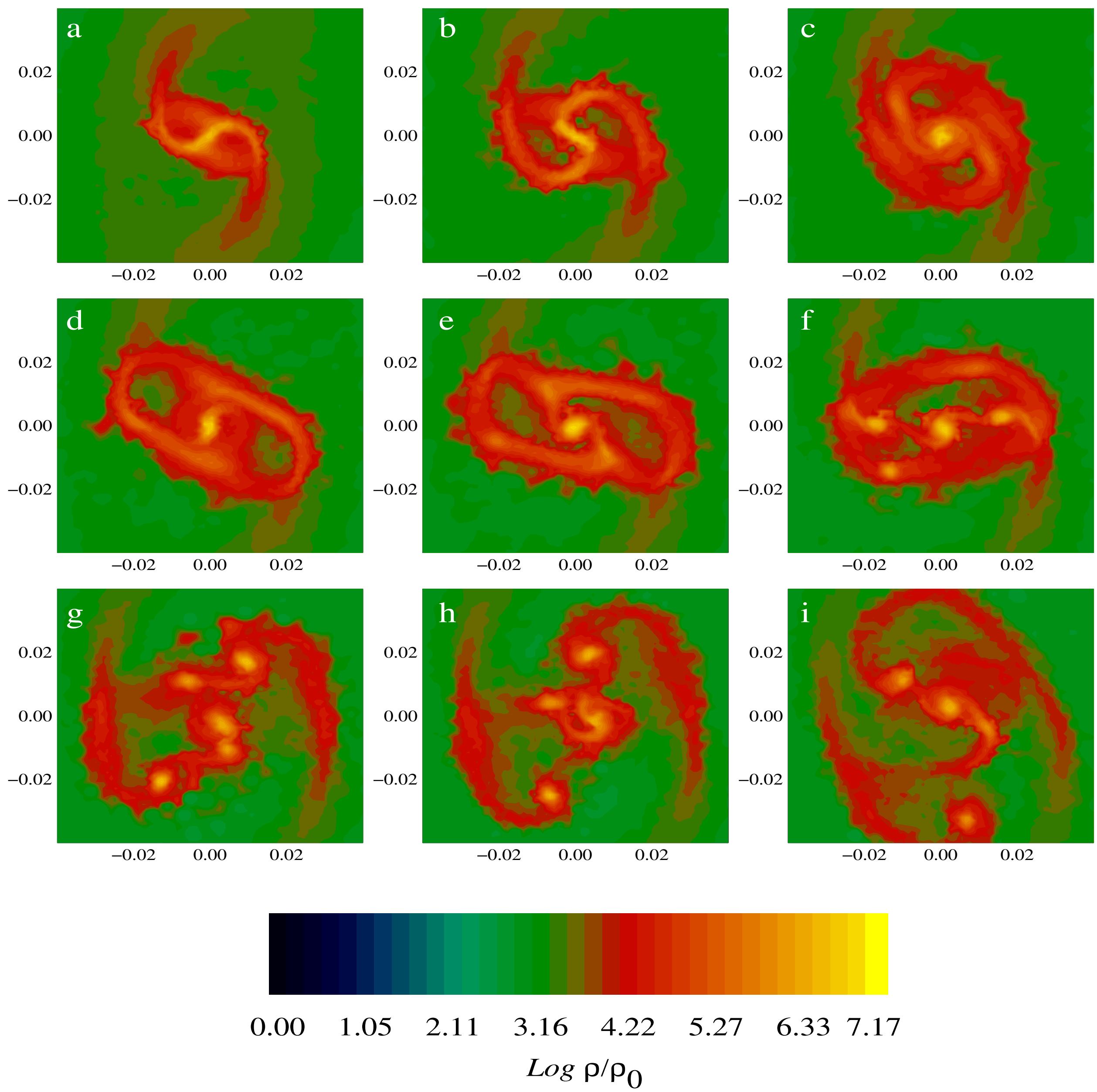

Fig. 14. Isodensity curves of the cloud mid-plane for model GB when the distribution of particles reaches a peak density of (a)$\rho_{\max} = 2.1569949 \times 10^{-11}$ g cm^{-3} at time $t/t_{\rm ff} = 0.680639$; (b)$\rho_{\max} = 3.2251779 \times 10^{-11}$ g cm^{-3} at time $t/t_{\rm ff} = 0.694144$; (c)$\rho_{\max} = 4.2332077 \times 10^{-11}$ g cm^{-3} at time $t/t_{\rm ff} = 0.699546$; (d)$\rho_{\max} = 5.9035415 \times 10^{-11}$ g cm^{-3} at time $t/t_{\rm ff} = 0.704948$; (e)$\rho_{\max} = 7.0227583 \times 10^{-11}$ g cm^{-3} at time $t/t_{\rm ff} = 0.708549$; (f)$\rho_{\max} = 7.4701831 \times 10^{-11}$ g cm^{-3} at time $t/t_{\rm ff} = 0.715751$; (g)$\rho_{\max} = 8.6511223 \times 10^{-11}$ g cm^{-3} at time $t/t_{\rm ff} = 0.725655$; (h)$\rho_{\max} = 1.0928224 \times 10^{-10}$ g cm^{-3} at time $t/t_{\rm ff} = 0.729256$; and (i)$\rho_{\max} = 1.2554817 \times 10^{-10}$ g cm^{-3} at time $t/t_{\rm ff} = 0.737359$.

Then, for the simulation UA, in which the thermodynamical change occurs earlier, the resulting fragments are bigger and more massive than in the other uniform models runs, where the change occurs later. The filament entirely disappears only for model UA, whereas it persists for the others.

The uniform models are therefore a very illustrative example of prompt fragmentation producing a binary protostellar system.

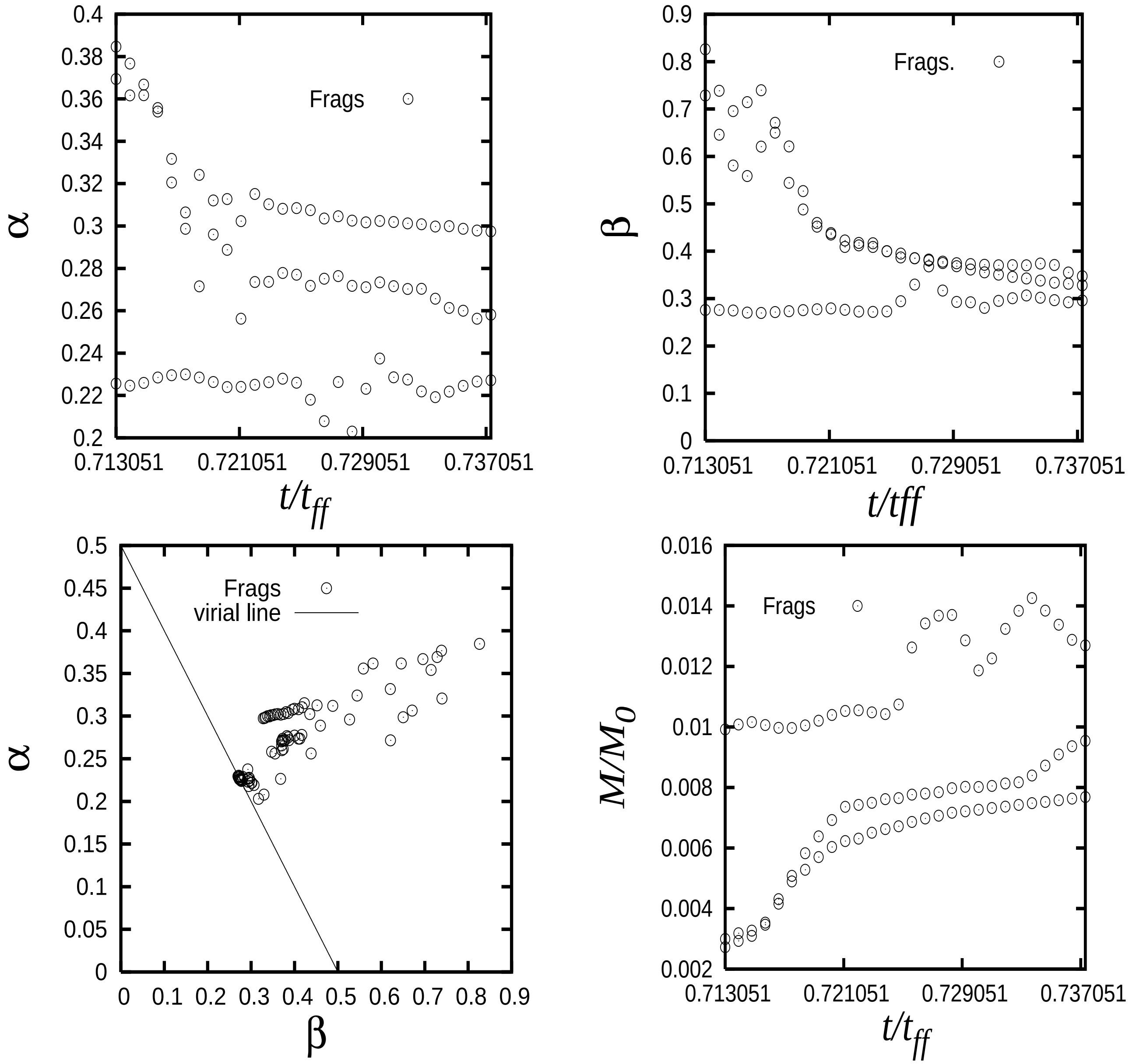

Fig. 15. Integral properties for the fragments found in models *GB*.

4.2. *The Gaussian Cloud*

Our simulations of the Gaussian cloud can follow the collapse to the maximum densities and times shown in Table 4. The properties of the fragments, the mass, the radius, the α and β ratios are shown in Table 5.

For Gaussian models we note that the effects of considering the non-ideal nature of the collapse are more significant than for the uniform cloud. Small values of $\rho_{\rm crit}$ (heating of the gas is taken into account earlier in the collapse) can indeed result in more fragmentation of the cloud. For instance, in model *GA* and *GB* we observe the appearance of up to 4 fragments while in models *GC* and *GD* fragmentation is less favored. However, in the former couple of models the occurrence of merging between fragments leaves us with only two final protostellar cores.

Let us now compare our results with the literature. Burkert & Bodenheimer (1996) considered the ideal collapse of the Gaussian cloud using the technique of nested grids. What these authors reported

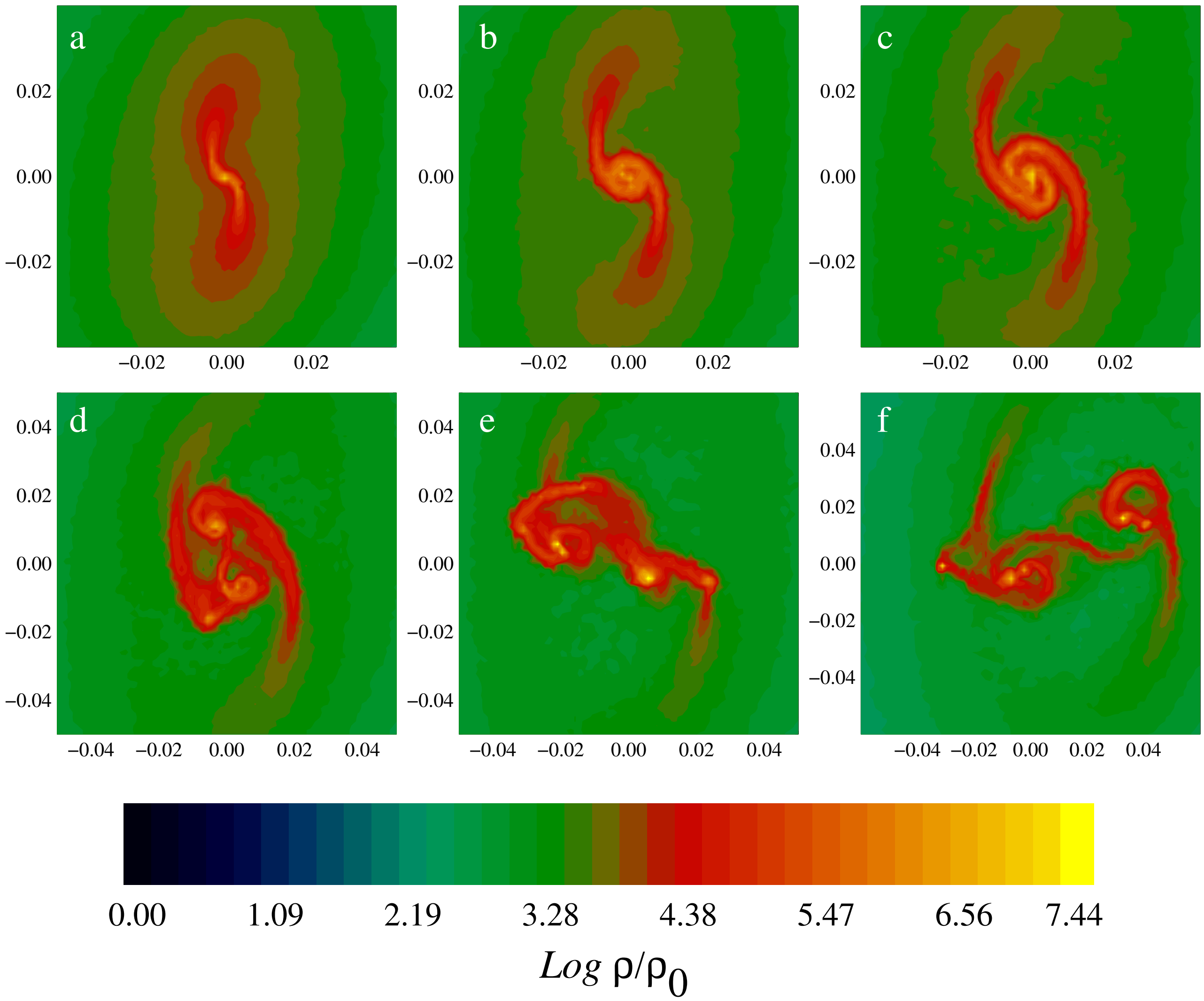

Fig. 16. Isodensity curves of the cloud mid-plane for model GC when the distribution of particles reaches a peak density of (a)$\rho_{\max} = 1.3574624 \times 10^{-10}$ g cm^{-3} at time $t/t_{\rm ff} = 0.657231$; (b)$\rho_{\max} = 4.2892007 \times 10^{-10}$ g cm^{-3} at time $t/t_{\rm ff} = 0.666234$; (c)$\rho_{\max} = 7.7961247 \times 10^{-10}$ g cm^{-3} at time $t/t_{\rm ff} = 0.675237$; (d)$\rho_{\max} = 3.7783788 \times 10^{-09}$ g cm^{-3} at time $t/t_{\rm ff} = 0.693244$; (e)$\rho_{\max} = 9.0149908 \times 10^{-09}$ g cm^{-3} at time $t/t_{\rm ff} = 0.711250$ and (f)$\rho_{\max} = 1.3768666 \times 10^{-08}$ g cm^{-3} at time $t/t_{\rm ff} = 0.729256$.

TABLE 2

MAXIMUM EVOLUTION TIME AND DENSITY FOR UNIFORM CLOUD MODELS

Model	UA	UB	UC	UD
$t_{\max}/t_{\rm ff}$	1.526036	1.338320	1.291054	1.276649
$\rho_{\max}$ g cm^{-3}	$2.3075786 \times 10^{-11}$	$6.8565254 \times 10^{-10}$	$5.9576158 \times 10^{-09}$	$2.8596622 \times 10^{-07}$

as a result of a simulation considered to be of "moderate resolution", is a system of three fragments that enter into orbit without merging; they distinguished a central fragment and two additional ones which they refer to as the exterior binary system (see Figures 1 and 2 in Burket & Bodenheimer 1996).

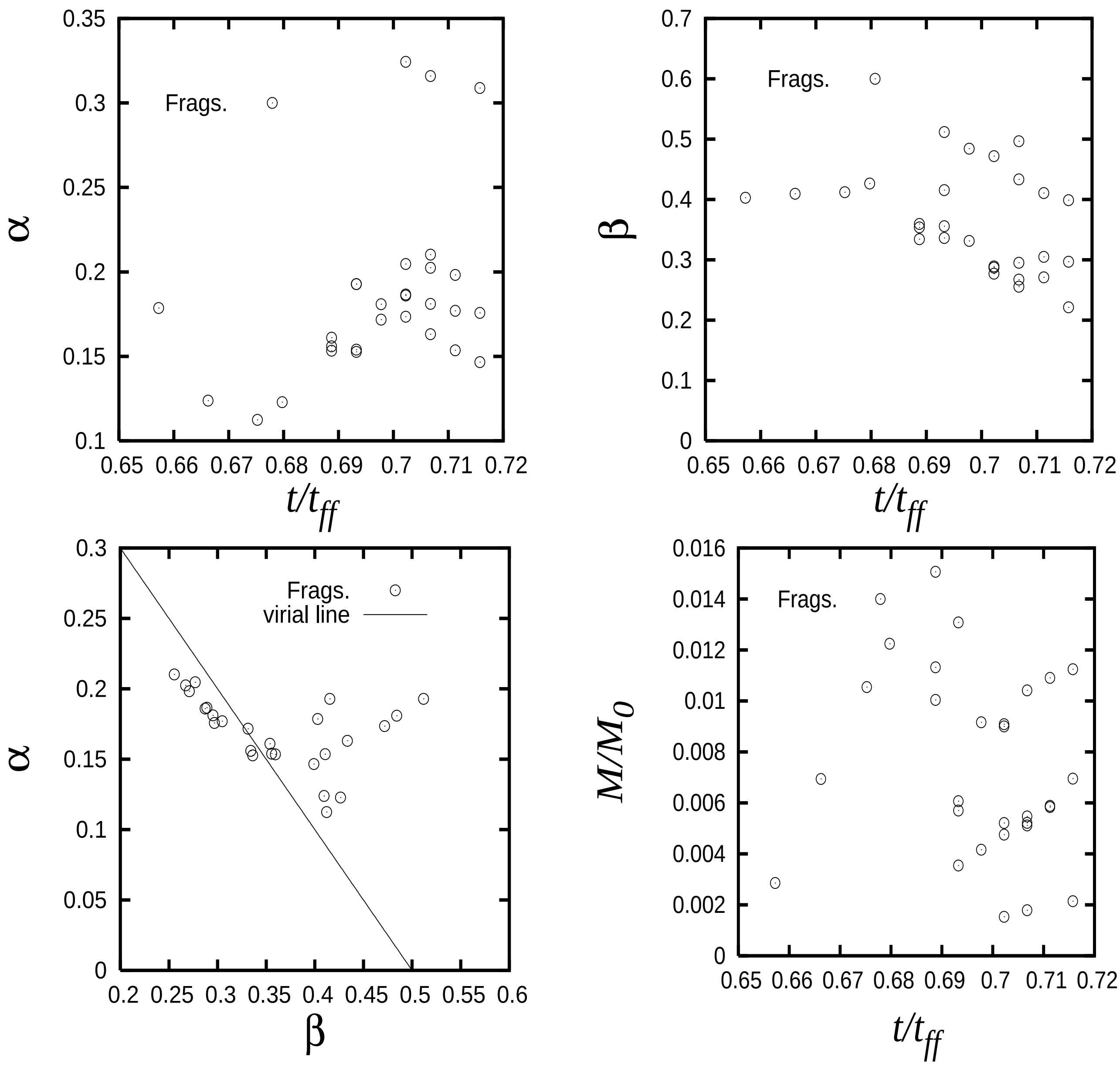

Fig. 17. Integral properties for the fragments found in models *GC*.

In the simulation that Burkert & Bodenheimer (1996) considered of "high resolution", they reported that the fragment located at the center divides in its turn provoking the appearance of an internal binary system. For this reason, they concluded that their simulation produced 4 fragments in orbit.

It is interesting to point out that results very similar to the ones of Burkert & Bodenheimer (1996) were observed in our model *GD*; for instance, compare our Figure 18a with their Figure 3c and our Figure 18d with their Figure 3f. In these simulations we never observed the fragmentation of the central clump.

In Boss et al. (2000) the Gaussian collapse was calculated with the Adaptive Mesh Refinement(AMR), a technique in which the AMR algorithm creates finer grids in order to achieve higher resolution where needed.

It is noteworthy that Boss et al. (2000) also observed the formation of well defined dense cores on the extremes of the central bar. They also noticed a

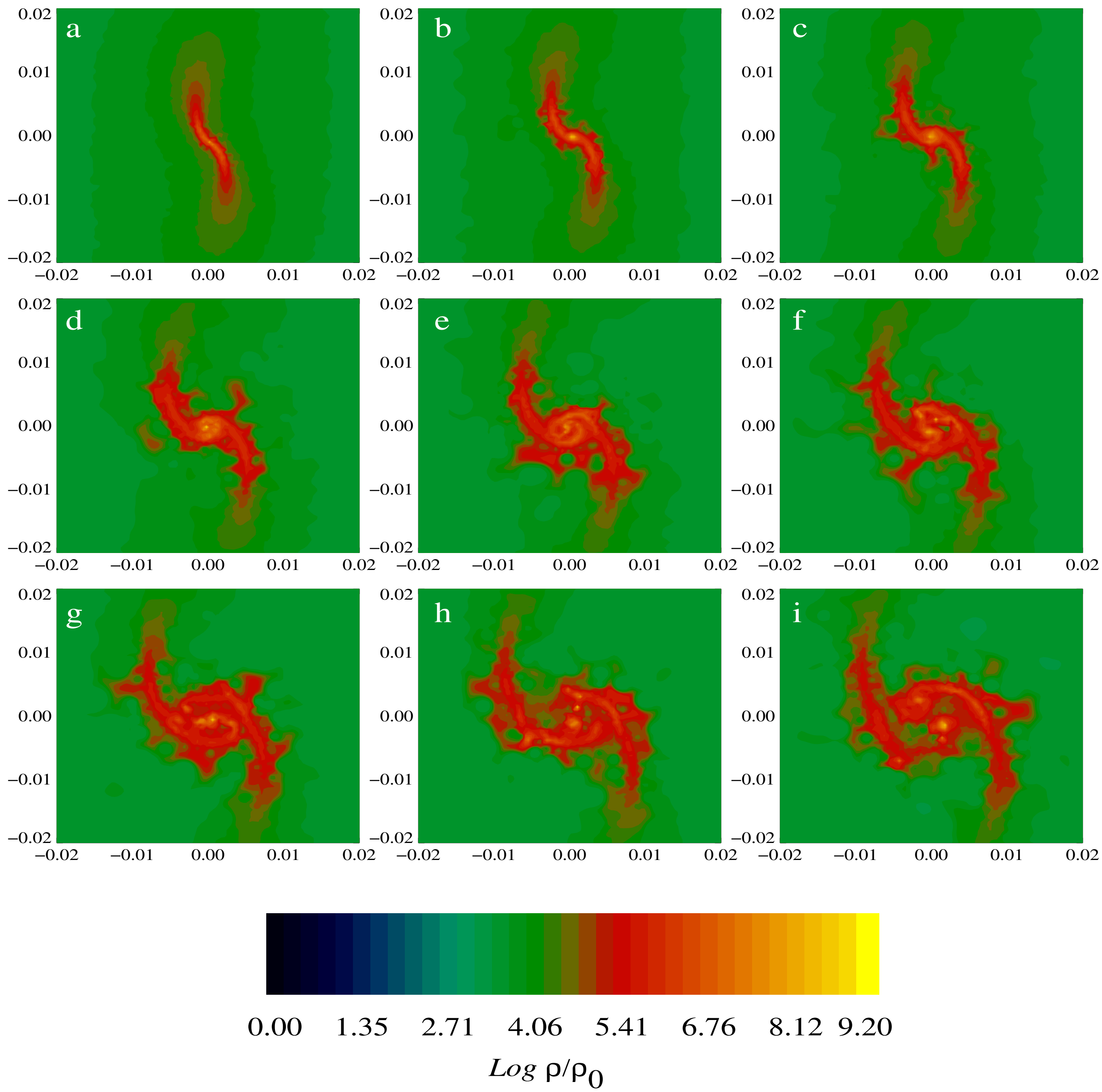

Fig. 18. Isodensity curves of the cloud mid-plane for model *GD* when the distribution of particles reaches a peak density of (a)$\rho_{\rm max} = 2.4750879 \times 10^{-09}$ g cm^{-3} at time $t/t_{\rm ff} = 0.654530$; (b)$\rho_{\rm max} = 8.7291514 \times 10^{-09}$ g cm^{-3} at time $t/t_{\rm ff} = 0.656331$; (c)$\rho_{\rm max} = 1.1161107 \times 10^{-08}$ g cm^{-3} at time $t/t_{\rm ff} = 0.658131$; (d)$\rho_{\rm max} = 1.9224208 \times 10^{-08}$ g cm^{-3} at time $t/t_{\rm ff} = 0.660832$; (e)$\rho_{\rm max} = 2.5560963 \times 10^{-08}$ g cm^{-3} at time $t/t_{\rm ff} = 0.662633$; (f)$\rho_{\rm max} = 3.3774650 \times 10^{-08}$ g cm^{-3} at time $t/t_{\rm ff} = 0.664433$; (g)$\rho_{\rm max} = 4.4997205 \times 10^{-08}$ g cm^{-3} at time $t/t_{\rm ff} = 0.666234$; (h)$\rho_{\rm max} = 6.3509960 \times 10^{-08}$ g cm^{-3} at time $t/t_{\rm ff} = 0.668035$ and (i)$\rho_{\rm max} = 8.4127299 \times 10^{-08}$ g cm^{-3} at time $t/t_{\rm ff} = 0.669835$.

fragmentation of the bar but only for the model in which they implemented the full Eddington approximation. They argued that the barotropic equation of state (which is the same equation we use in this work, see equation 9) is an approximation to the full Eddington model. They reported that the bar rapidly decayed into a single central clump surrounded by spiral arms.

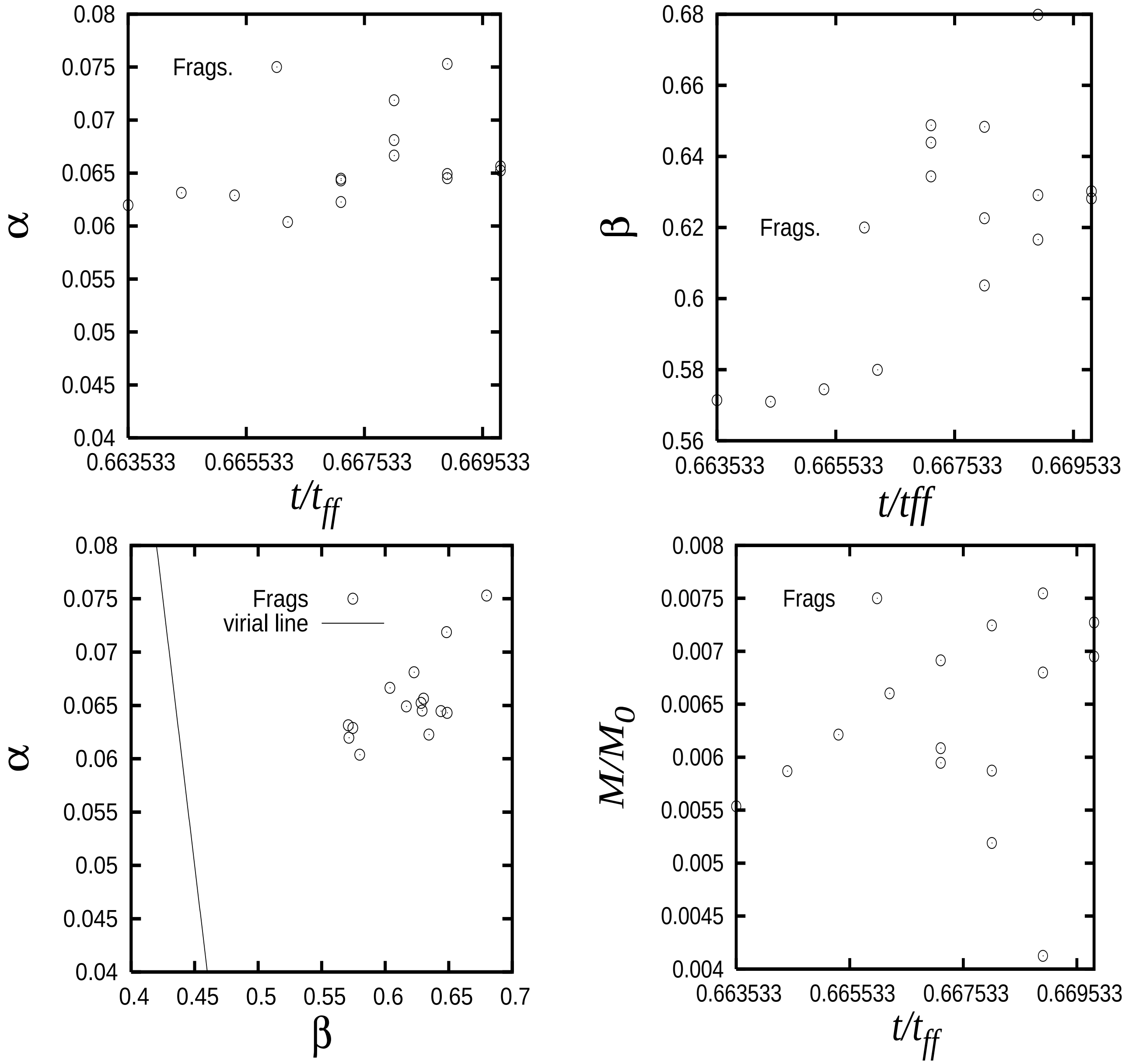

Fig. 19. Integral properties for the fragments found in models *GD*.

GA would like to thank ACARUS-UNISON for the use of their computing facilities and Ruslan Gabbasov for a very timely assistance in the making of this paper.

APPENDIX A
A NUMERICAL DEFINITION OF A FRAGMENT

In order to calculate the integral properties of protostellar cores we need a numerical definition of a resulting fragment. In our models we proceed as follows:

1. We locate the center of the fragment, that is, the particle with the highest density in a region (of the slice of matter surrounding the equator of the cloud) where the fragment is located.

2. Once the location of the center has been determined, we find all the particles which have density above or equal to some minimum density value within a given maximum radius from the center. This set of particles define the fragment and therefore its integral properties, for instance, its mass.

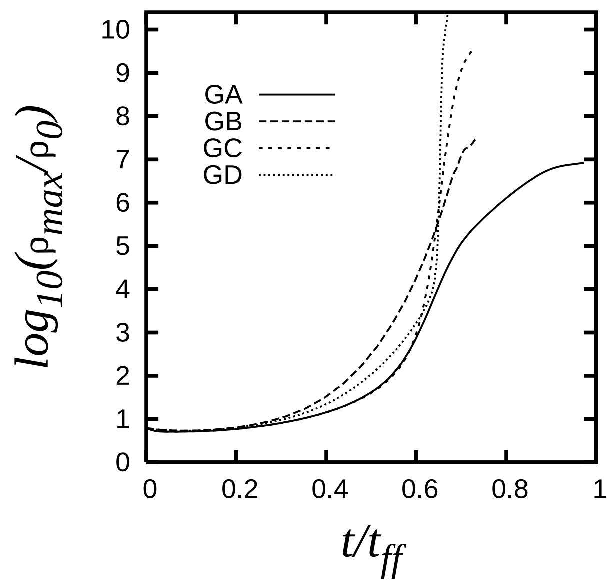

Fig. 20. Time evolution of the peak density for Gaussian models.

TABLE 3

PHYSICAL PROPERTIES OF THE RESULTING FRAGMENTS FOR THE UNIFORM CLOUD

Model	Time ($t_{\rm ff}$)	$M_{\rm f}/M_0$	$\|\alpha\|$	$\|\beta\|$
UA	1.440506	0.094811	0.248363	0.285593
		0.092660	0.252887	0.262221
UB	1.319864	0.070219	0.314145	0.283510
		0.064592	0.258661	0.320606
		0.008509	0.569961	0.063677
UC	1.289253	0.047144	0.224965	0.364621
		0.047158	0.223713	0.382579
UD	1.277099	0.021195	0.201898	0.326431
		0.019875	0.219058	0.323086

TABLE 4

MAXIMUM EVOLUTION TIME AND DENSITY FOR GAUSSIAN CLOUD MODELS

Model	GA	GB	GC	GD
$t_{\max}/t_{\rm ff}$	0.972342	0.737359	0.729256	0.669835
$\rho_{\max}$ g cm^{-3}	$3.1654053 \times 10^{-11}$	$1.2554817 \times 10^{-10}$	$1.3768666 \times 10^{-08}$	$8.4127299 \times 10^{-08}$

3. To calculate the ratios of energy (the α and β defined in § 2.2) for a given fragment, a length h is required for each simulation particle in the fragment in order to locate its neighboring particles. We use the prescription that $h \approx R_0/\left(2\, N_f\right)^{\frac{2}{3}}$ where N_f is the number of particles defining the fragment. However, we cannot assure that the number of neighbors of each particle is always 40.

TABLE 5

PHYSICAL PROPERTIES OF THE RESULTING FRAGMENTS FOR THE GAUSSIAN CLOUD

Model	Time ($t_{\rm ff}$)	$M_{\rm f}/M_0$	$\vert\alpha\vert$	$\vert\beta\vert$
GA	0.936329	0.053970	0.280301	0.238896
		0.053171	0.247702	0.247702
GB	0.737359	0.012697	0.227151	0.296011
		0.009542	0.258132	0.347152
		0.007682	0.297418	0.327948
GC	0.688742	0.015067	0.155920	0.334231
		0.011323	0.161015	0.353868
		0.010044	0.153414	0.359508
GC	0.715751	0.011245	0.175698	0.296750
		0.006952	0.146549	0.398985
		0.002143	0.308841	0.221144
GD	0.669835	0.007273	0.065245	0.628165
		0.006951	0.065631	0.630207

REFERENCES

Arreaga, G., Klapp, J., Sigalotti, L., & Gabbasov, R. 2007, ApJ, 666, 290
Balsara, D. S. 1995, J. Comput. Phys., 121, 357
__________. 2001, J. Korean Astron. Soc., 34, S181
Bate, M. R., & Burkert, A. 1997, MNRAS, 288, 1060
Boden, A. F. 2005, ApJ, 635, 442
Bodenheimer, P., Burkert, A., Klein, R. I. & Boss, A. P. 2000, in Protostars and Planets IV, ed. V. G. Mannings, A. P. Boss, & S. S. Russell (Tucson: University of Arizona Press), 675
Boss, A. P. 1991, Nature, 351, 298
Boss, A. P., & Bodenheimer, P. 1979, ApJ, 234, 289
Boss, A. P., Fisher, R. T., Klein, R., & McKee, C. F. 2000, ApJ, 528, 325
Burkert, A., & Bodenheimer, P. 1993, MNRAS, 264, 798
__________. 1996, MNRAS, 280, 1190
Gabbasov, R. F., Rodríguez-Meza, M. A., Klapp, J., & Cervantes-Cota, J. L. 2006, A&A, 449, 1043
Kitsionas, S., & Whitworth, A. P. 2002, MNRAS, 330, 129
Mathieu, R. 1994, ARA&A, 32, 465
Monaghan, J. J. 1997, J. Comput. Phys., 136, 298
__________. 2005, Rep. Prog. Phys., 68, 1703
Monaghan, J. J., & Gingold, R. A. 1983, J. Comput. Phys., 52, 374
Myers, P. C. 1983, Fragmentation of Molecular Cores and Star Formation, ed. E. Falgarone, F. Boulanger, & G. Duvert (Dordrecht: Kluwer), 221
Nelson, A. F. 2006, MNRAS, 373, 1039
Sigalotti, L., & Klapp, J. 2001, Int. J. Mod. Phys. D, 10, 115
Springel, V. 2005, MNRAS, 364, 1105
Tohline, J. E. 2002, ARA&A, 40, 349
Truelove, J. K., Klein, R. I., McKee, C. F., Holliman, J. H., Howell, L. H., & Greenough, J. A. 1997, ApJ, 489, L179
Whitehouse, S. C., & Bate, M. R. 2006, MNRAS, 367, 32

Guillermo Arreaga-García and Julio Saucedo-Morales: Centro de Investigación en Física, Universidad de Sonora, México, Apdo. Postal 14740, C.P. 83000, Hermosillo, Sonora, Mexico (garreaga, jsaucedo@cajeme.cifus.uson.mx).
Juan Carmona-Lemus and Ricardo Duarte-Pérez: Gerencia de Sistemas, Instituto Nacional de Investigaciones Nucleares, Carretera México-Toluca, Ocoyoacac C.P. 52750, Estado de México, Mexico (jcl, rdp@nuclear.inin.mx).